

**Unravelling Polymorphism-Driven Luminescence in GFP Chromophore Analogues:  
Insights into Phase Transition and Morphology-Dependent Optical Waveguide  
Properties**

Niteen B. Dabke,<sup>a</sup> Yash Raut,<sup>a</sup> Bhupendra P. Mali,<sup>a</sup> Rinu Pandya,<sup>a</sup> Kumar Vanka,<sup>ab</sup>

Kochunnoony Manoj<sup>c</sup> and Rajesh G. Gonnade<sup>ab\*</sup>.

<sup>a</sup>Physical & Materials Chemistry Division, CSIR-National Chemical Laboratory, Dr. Homi Bhabha Road, Pashan, Pune, Maharashtra, 411008, India.

<sup>b</sup>Academy of Scientific and Innovative Research (AcSIR), Sector 19, Kamla Nehru Nagar, Ghaziabad, Uttar Pradesh, 201002, India.

<sup>c</sup>Institution Research and Development Laboratory, Alchemy Innovative Solutions Kochi, Kerala 683544, India.

Correspondence author email: [rg.gonnade@ncl.res.in](mailto:rg.gonnade@ncl.res.in)

## Contents:

Experimental Section .....	6
Scheme S1. Synthetic route for compounds A and B .....	11
Figure S1. <sup>1</sup> H NMR spectrum of a compound A in CDCl <sub>3</sub> .....	13
Figure S2. <sup>13</sup> C NMR spectrum of a compound A in CDCl <sub>3</sub> .....	14
Figure S3. Mass spectrum of a compound A. ....	15
Figure S4. <sup>1</sup> H NMR spectrum of a compound B in CDCl <sub>3</sub> . ....	16
Figure S5. <sup>13</sup> C NMR spectrum of a compound B in CDCl <sub>3</sub> .....	17
Figure S6. Mass spectrum of a compound B. ....	18
Table S1. Crystallization of compound A polymorphs from various common organic solvents by slow evaporation method. ....	19
Table S2. Crystallization of compound B polymorphs from various common organic solvents by slow evaporation method.....	20
Figure S7. Photomicrograph of crystals of polymorphs of A and B obtained concomitantly, (a) Form A1 (plates) and Form A2 (needles), (b) Form B1 (needles) and Form B2 (plates). ....	21
Table S3. Single crystal X-ray diffraction data for polymorphs of compound A and B.....	22
Figure S8. The Oak Ridge Thermal Ellipsoid Plots (ORTEPs) of (a) Form A1, (b) Form A2, (c) Form B1 and (d) Form B2 drawn at the 50% ellipsoid probability level and hydrogen atoms are displayed as small spheres with radii 0.07 Å and (e) and (f) are the structure overlay of polymorphs (Forms A1 & A2 and Forms B1 & B2) of compounds A and B, respectively.....	23
Figure S9. Face indices image of Form A1 crystal. ....	24
Figure S10. Face indices image of Form A2 crystal.....	24
Table S4. Geometrical parameters of intermolecular interactions in all the polymorphs of A.....	25
Figure S11. Visualization of energy frameworks showing electrostatic (red), dispersion (green) components and total interaction energy (blue) for Form A1, in the (a) (100), (b) (010) and (c) (001) faces, respectively. The energy threshold is 5 kJ mol <sup>-1</sup> . ....	26
Table S5. Interaction energy based on energy frameworks for Form A1 crystals.....	27
Figure S12. Visualization of energy frameworks showing electrostatic (red), dispersion (green) components and total interaction energy (blue) for Form A2, in the (a) (100), (b) (010) and (c) (001) faces, respectively. The energy threshold is 5 kJ mol <sup>-1</sup> . ....	28
Table S6. Interaction energy based on energy frameworks for Form A2 crystals.....	29
Table S7. Geometrical parameters of intermolecular interactions in all the polymorphs of B. ....	30
Figure S13. Face indices image of Form B1 crystal. ....	31
Figure S14. Visualization of energy frameworks showing electrostatic (red), dispersion (green) components and total interaction energy (blue) for Form B1, in the (a) (100), (b) (010) and (c) (001) faces, respectively. The energy threshold is 5 kJ mol <sup>-1</sup> . ....	32
Table S8. Interaction energy based on energy frameworks for Form B1 crystals. ....	33
Figure S15. Face indices image of Form B2 crystal. ....	33

Figure S16. Visualization of energy frameworks showing electrostatic (red), dispersion (green) components and total interaction energy (blue) for Form B2, in the (a) (100), (b) (010) and (c) (001) faces, respectively. The energy threshold is 5 kJ mol <sup>-1</sup> .	34
Table S9. Interaction energy based on energy frameworks for Form B2 crystals.	35
Figure S17. H-aggregation (head-to-head) of molecules in Form A1 (a) and Form B1 (b) and J-aggregation (head-to-tail) of molecules in Form A2 (c) and Form B2 (d).	36
Figure S18. Hirshfeld surfaces for (a) Form A1, (b) Form A2, (c) Form B1 and (d) Form B2, and (e), (f), (g) and (h) are fingerprint plots of the Hirshfeld surfaces for Form A1, A2, B1 & B2 respectively.	37
Figure S19. The contributions of various intermolecular interactions to Hirshfeld surfaces areas in Form A1 and Form A2 polymorphs of A.	38
Figure S20. The contributions of various intermolecular interactions to Hirshfeld surfaces areas in Form B1 and Form B2 polymorphs of B.	39
Figure S21. Overlay of the PXRD patterns of the polymorphs of (a) compound A and (b) compound B.	40
Figure S22. Overlay of experimental (black) and calculated (red) powder X-ray diffraction patterns of (a) Form A1, (b) Form A2, (c) Form B1 and (d) Form B2 crystals.	41
Figure S23. DSC thermograms for all the polymorphs of A.	42
Figure S24. DSC thermogram of Form A2 crystals.	42
Figure S25. DSC thermograms for all the polymorphs of B.	43
Figure S26. DSC thermogram of Form B2 crystals.	43
Figure S27. Photomicrographs of Form A1 crystals captured during its phase transition to Form A2 crystals over HSM studies.	44
Figure S28. Photomicrographs of Form A2 crystals captured during HSM study.	45
Figure S29. Photomicrographs of Form B1 crystals captured during its phase transition to Form B2 crystals over HSM studies.	46
Figure S30. Photomicrographs of Form B2 crystals captured during HSM study.	47
Figure S31. VT-PXRD profiles of Form A1 crystals recorded at different temperatures.	48
Figure S32. VT-PXRD profiles of Form A2 crystals recorded at different temperatures.	49
Figure S33. VT-PXRD profiles of Form B1 crystals recorded at different temperatures.	50
Figure S34. VT-PXRD profiles of Form B2 crystals recorded at different temperatures.	51
Figure S35. Graphical representation of solvent vapour fuming experiment.	52
Figure S36. The schematic representation of E-Z flipping of GFP chromophore analog A.	53
Figure S37. The schematic representation of E-Z flipping of GFP chromophore analog B.	53
Figure S38. Normalized absorption (solid lines) and fluorescence (broken lines) spectra (excited at 360 nm) for, (a-b) compound A and (c-d) compound B in common organic solvents (C = 20 x 10 <sup>-5</sup> M).	54
Figure S39. Room temperature time-resolved PL decay curves for (a) compound A and (b) compound B in common organic solvents (C = 20 x 10 <sup>-5</sup> M).	55

Table S10. Absorption maxima, emission maxima, quantum yield (%), and fluorescence lifetime measurement for compound A in common organic solvents ( $C = 20 \times 10^{-5} \text{ M}$ ).....	56
Table S11. Absorption maxima, emission maxima, quantum yield (%), and fluorescence lifetime measurement for compound B in common organic solvents ( $C = 20 \times 10^{-5} \text{ M}$ ).....	57
Figure S40. The CIE coordinates position on chromaticity for emission of the polymorph A1 (yellow star), A2 (green star), B1 (pink star) and B2 (blue star) in the crystalline state.....	58
Figure S41. Room temperature time-resolved PL decay curves for compound A and B (a) A in Ethanol solution, (b) B in Ethanol solution, (c) for polymorphs of A and (d) for polymorphs of B.....	59
Table S12. Absorption maxima, emission maxima, quantum yield (%), and fluorescence lifetime measurement for the polymorphs of compound A and B in the solid-state.....	60
Figure S42. (a) Normalized fluorescence spectra (excited at 360 nm) for Form A1 recorded at different temperatures, (b) CIE coordinates position on chromaticity for emission of Form A1 at 25°C (red star) and at 100°C (blue star) in the crystalline state.....	61
Figure S43. (a) Normalized fluorescence spectra (excited at 360 nm) for Form B1 recorded at different temperatures, (b) CIE coordinates position on chromaticity for emission of Form B1 at 25°C (blue star) and at 125°C (pink star) in the crystalline state.....	62
Figure S44. Photomicrographs captured under UV light for the polymorphs of compound A and B, (a) Form A1, (b) Form A2, (c) Form B1 and (d) Form B2.....	63
Figure S45. Normalized solid-state absorption and fluorescence spectra (excited at 360 nm) for (a-b) Form A2 and (c-d) for Form B1 respectively.....	64
Figure S46. Room temperature time-resolved PL decay curves for Form A2 and Form B1, before and after grinding.....	65
Table S13. Absorption maxima, emission maxima, quantum yield (%), and fluorescence lifetime measurement for Form A2 and Form B1 in the solid-state.....	66
Figure S47. Overlay of powder X-ray diffraction patterns of (a) Form A1, (b) Form A2, (c) Form B1 and (d) Form B2.....	67
Figure S48. Overlay of DSC thermograms for, (a) Form A1, (b) Form A2, (c) Form B1 and (d) Form B2 in crystalline and powdered state.....	68
Figure S49. Overlay of experimental and calculated powder X-ray diffraction patterns of Form B1 recorded at different temperatures.....	69
Figure S50. Structure overlay of Form B1 collected at 25 °C (yellow) and 80 °C (green).....	69
Calculations of Photophysical Parameters.....	70
Bandgap calculations:.....	70
Figure S51. Tauc plot of UV-visible absorption data for the calculation of band-gap energy of all the polymorphs of A and B (a) Form A1, (b) Form A2, (c) Form B1 and (d) Form B2.....	71
Figure S52. Frontier molecular orbitals and their corresponding energy levels are calculated using the Gaussian 09 program by employing the B3LYP/6-311 <sup>++</sup> G(d,p) level of theory. (a) Form A1, (b) Form A2, (c) Form B1 and (d) Form B2.....	72
Table S14. Band gap and transition values corresponding to the $\lambda_{\text{max}}$ . ( $f$ = oscillator strength).....	73
Figure S53. Ethanol-based anti-counterfeiting ink was prepared from Form A1 and observed under the (a) UV light (b) visible light and (c) UV light after heating to 140°C.....	74



..... 74

Figure S54. Ethanol-based anti-counterfeiting ink prepared from Form B1 under the (a) UV light, (b) visible light, and (c) UV light after heating to 140°C..... 74

References..... 75

## Experimental Section

### 1. Single-Crystal X-Ray Diffraction Studies

Good-quality single crystals of each polymorph suitable for single-crystal X-ray diffraction analysis were selected using a Leica polarizing microscope (S8 APO). The X-ray intensity data for each polymorph were measured on a Bruker D8 VENTURE Kappa Duo PHOTON II CPAD diffractometer equipped with a Mo micro-focus sealed X-ray tube [ $\lambda$  (Mo  $K\alpha$ ) = 0.71073 Å, generator power 50 kV and 1.4 mA] and Incoatech multilayer mirror optics. All data collections were conducted at 100 (2) K. A preliminary set of cell constants and an orientation matrix were calculated from a total of 36 frames (matrix, three runs, each run comprised of 12 frames). The full-intensity data were collected using an optimized strategy that consisted of different sets of  $\omega$ ,  $\psi$  and  $2\theta$  with 0.5° frame width, with the sample-to-detector distance fixed at 5.00 cm with varying exposure time (10–20 s) depending on the diffraction power of the crystals. The whole process of X-ray data acquisition (unit-cell measurements and data collection) was controlled and monitored by the APEX3 program suite (Bruker, 2016).<sup>1</sup> The complete data sets were corrected for Lorentz–polarization and absorption effects (multi-scan method) using SAINT and SADABS programs with the transmission coefficients. Using the APEX3 (Bruker, 2016) program suite,<sup>1</sup> the structure was solved with the SHELXS97 (Sheldrick, 2008) structure solution program using direct methods.<sup>2</sup> The model was refined with a version of SHELXL-2013 (Sheldrick, 2015) using least-squares minimization based on  $F^2$ .<sup>3</sup> All non-hydrogen atoms were refined anisotropically. On the other hand, hydrogen atoms were refined isotropically by placing them in a geometrically idealized position and constraining them to ride on their parent atoms. ORTEP (Farrugia, 2012) views of all the polymorphs were drawn with 50% probability displacement ellipsoids and H atoms are shown as small spheres of arbitrary radii.<sup>4</sup> The molecular packing diagrams were generated using the

Mercury program (Macrae et al., 2020).<sup>5</sup> Geometric calculations were performed using SHELXTL (Bruker, 2016)<sup>1</sup> and PLATON (Spek, 2020).<sup>6</sup>

## **2. Lattice Energy Calculations and Hirshfeld Surface Analysis**

The lattice energies of all the polymorphs were estimated using the classical Atom-Atom Coulomb–London–Pauli (AA-CLP) model embedded in the CLP package.<sup>7</sup> The energy values of the intermolecular potentials were estimated using the UNI-force field model integrated into the program Mercury.<sup>5,8,9</sup> Intermolecular interactions in compounds **A** and **B** were quantified via Hirshfeld surface analysis<sup>10</sup> using CrystalExplorer v 3.1.<sup>11</sup> All the intermolecular interactions involved in the polymorphs were evaluated concerning their contribution to the overall stability of the crystal structure. The Hirshfeld surfaces and fingerprint plots<sup>12</sup> were plotted to compare the differences in the intermolecular interactions between the different forms. Further, Crystal Explorer was also used for interaction energy calculations and energy framework of polymorphs.<sup>13</sup> For the calculation, a cluster of radius 3.8 Å was generated around the central molecule. The total interaction energy ( $E_{\text{tot}}$ ) was estimated after taking into account the electrostatic ( $E_{\text{ele}}$ ), polarization ( $E_{\text{pol}}$ ), dispersion ( $E_{\text{dis}}$ ), and exchange-repulsion ( $E_{\text{rep}}$ ) energy contributions. The calculations were performed based on their crystal geometries using the B3LYP hybrid functional and the 6-311G (d,p) basis sets.

## **3. Powder X-Ray Diffraction Studies**

All polymorph's powder X-ray diffraction was analysed using Bruker's D8 VENTURE single-crystal X-ray diffractometer. A small amount of the sample was ground to a fine powder using a mortar and pestle and placed in a Lindeman capillary (0.7 mm diameter), which was then mounted on the diffractometer. The sample-to-detector distance was fixed at 230 mm, and angles  $\varphi$  and  $\chi$  were set at 0°, 6° and -6° for different  $\theta$  values; for example, angles  $\omega$  set at 6° for  $\theta$  values ranging from 12° to 48° (in intervals of 12°) and angles  $\omega$  set at -6° for  $\theta$  values

ranging from  $-12^{\circ}$  to  $-48^{\circ}$  (in intervals of  $12^{\circ}$ ). Intensity measurements were carried out at room temperature with a Cu microfocus sealed tube diffraction source ( $\text{Cu K}\alpha = 1.54178 \text{ \AA}$ ). The sample was rotated uniformly to complete  $360^{\circ}$  and exposed for 120 s for all scans. After completing all scans, the Debye rings were integrated to create a raw file converted to an xrdml file using PowDLL Converter.<sup>14</sup> Finally, a PXRD graph with background correction was plotted using the xrdml file.

#### **4. Thermal Studies**

Thermal studies were conducted using differential scanning calorimetry (DSC) and hot-stage microscopy (HSM). DSC was performed on a Mettler Toledo DSC 822e instrument by measuring the enthalpy change. The crystals of all polymorphs were first air-dried to remove traces of solvent from the crystal surface. The dried crystals were then taken on an aluminium pan (volume:  $40 \mu\text{L}$ ) and crimped. The pan was heated from 298 K to 433 K at a rate of 3K/min, followed by a cooling cycle from 433 K to 298 K at a rate of 10 K/min, which was again followed by a second heating cycle with the same temperature range, using the empty aluminium pan as a reference. Nitrogen gas ( $40 \text{ mL/min}$ ) is used for purging. Liquid Nitrogen is used to cool the furnace. HSM studies were carried out on the Linkam heating stage (LTS 420) mounted on the Leica optical polarizing microscope (S8APO). Thermal microscopy was conducted by heating the crystals from room temperature at a 5 K/min heating rate. The images and videos were captured during the heating experiment using Leica Application Suite (LAS, v4.8) software.

#### **5. Solvent Vapor Fuming Experiment**

An experiment involving solvent vapor treatment was carried out with different solvents such as chloroform, dichloromethane, ethanol, and methanol. Crystals of the individual polymorphs were placed on a slide, which was then positioned over a beaker. This beaker

was placed within a larger beaker partially filled with the respective solvent, and the outer beaker's opening was sealed to prevent vapor from escaping. The entire setup was heated to 50 °C on a hot plate. Continuous monitoring under UV light was carried out at regular intervals to observe any changes in emission.

## **6. Photo Physical Measurements**

Absorption spectra were determined using a Labindia UV– Vis spectrophotometer (model UV 3092) with an automatic cell changer and high-intensity tungsten, halogen and deuterium lamp. Photoluminescence (PL) decay dynamics were recorded using a fluorescence spectrometer (Edinburgh Instruments, Model FS5 spectrofluorometer) using a microsecond flash lamp with a power of 100 W. For PL decay dynamics, the sample was excited at 360 nm using a microsecond flash lamp, whereas the excitonic PL decay was recorded using a 330 nm picosecond-pulsed LED laser source. The absolute quantum yield measurement was carried out using a Horiba Jobin Yvon Fluorolog 3 spectrofluorometer with the integrated quantum sphere.

## **7. Computational Studies**

DFT and TD-DFT calculations were performed on the crystal structure geometry of polymorphs using the Gaussian 09<sup>15</sup> program by employing the B3LYP<sup>16</sup>/6-311<sup>+</sup>2G(d,p) and B97D3<sup>17</sup>/6-311<sup>+</sup>2G(d,p) levels of theory to evaluate the HOMO–LUMO gap as well as to obtain insights into the UV-Vis spectra.

## **8. Wave guiding studies**

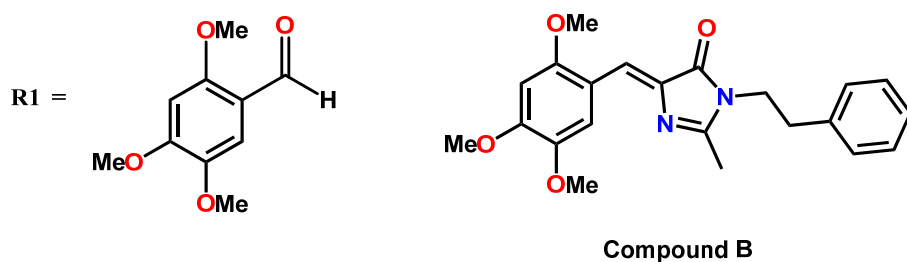
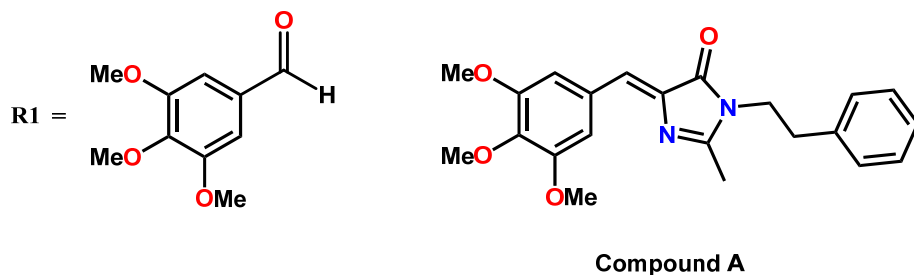
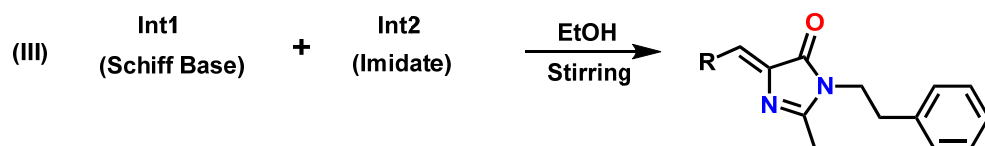
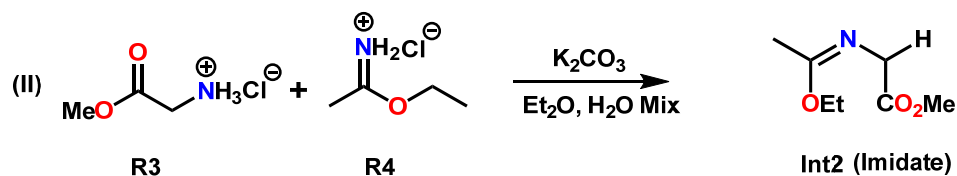
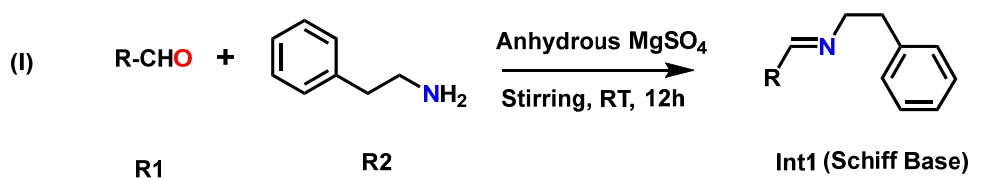
The experiments on optical waveguiding were conducted utilizing the Leica DMI8 laser confocal microscopy system, which is outfitted with a Leica HyD (Hybrid Detector technology) detector and a CMOS camera. A 405 nm continuous wave laser served as the excitation source. The emitted signal was captured using a 10x objective transmitted to the

HyD detector through an optical fibre, and the collected data were analyzed using the LasX software by Leica.

### **9. Fluorescent inks**

The preparation of fluorescent inks involves a simple procedure conducted through grinding, employing an aqueous solution of polyvinyl alcohol (PVA) as a medium. To prepare the aqueous PVA solution, 0.5 grams of PVA is dissolved in 10 mL of water and heated to approximately 80 °C for 2 hours. Following this, each polymorph is taken individually in a mortar pestle, and PVA solution is added and ground to obtain fluorescent ink.

**Scheme S1.** Synthetic route for compounds A and B



To synthesize the Schiff bases, the corresponding aldehyde (R1 = 1 mmol) and 2-phenylethylamine (R2 = 1.1 mmol) were combined in ethanol and the reaction was allowed to stir under ambient conditions for 12 hours. The synthesized imidate then mixed with the Schiff base for the (2+3) cycloaddition reaction. Under ambient conditions, overnight stirring of the reaction mixture typically led to the precipitation of a solid reaction product. The obtained

product is then purified by flash column chromatography with an ethyl acetate: petroleum ether (1:2) combination over silica gel (230–400 mesh).

#### **Synthesis of Compound A:**

**(2-methyl-3-phenethyl-5-(3,4,5-trimethoxybenzylidene)-3,5-dihydro-4H-imidazol-4-one**

**(Compound A):** m. p. 393-395 K; IR v:1688  $\text{cm}^{-1}$  (C=O);  $^1\text{H}$  NMR (400 MHz, Chloroform-d)  $\delta$  ppm: 1.94 (s, 3 H) 2.94 (s, 2 H) 3.82 (s, 2 H) 3.89 - 3.92 (m, 9 H) 7.01 (s, 1 H) 7.14 - 7.31 (m, 5 H) 7.47 (s, 2 H)  $^{13}\text{C}$  NMR (400 MHz, CHLOROFORM-d)  $\delta$  ppm: 15.42, 35.26, 42.73, 56.15, 60.98, 76.78, 77.04, 77.29, 109.54, 126.92, 127.11, 128.87, 128.97, 129.71, 137.91, 138.05, 140.18, 153.15, 162.09, 170.67 ppm; MS-SI (m/z) calcd. For  $\text{C}_{22}\text{H}_{24}\text{N}_2\text{O}_4$ : 380.43; found: 381.18 [ $\text{H}^+$ ]. For  $^1\text{H}$ ,  $^{13}\text{C}$  NMR and mass spectra, see [Figures S1-S3](#).

#### **Synthesis of Compound B:**

**(Z)-2-methyl-3-phenethyl-5-(2,4,5-trimethoxybenzylidene)-3,5-dihydro-4H-imidazol-4-**

**one (Compound B):** m. p. 395-397 K; IR v:1696  $\text{cm}^{-1}$  (C=O);  $^1\text{H}$  NMR (400 MHz, Chloroform-d)  $\delta$  ppm 1.92 (s, 3 H) 2.93 (t, 2 H) 3.80 (t, 2 H) 3.85 - 3.99 (m, 9 H) 6.47 (s, 1 H) 7.11 - 7.33 (m, 5 H) 7.63 (s, 1 H) 8.52 (s, 1 H)  $^{13}\text{C}$  NMR (400 MHz, CHLOROFORM-d)  $\delta$  ppm 15.30, 35.26, 42.57, 55.90, 56.25, 56.44, 76.69, 77.00, 77.32, 96.03, 114.88, 115.31, 121.20, 126.75, 128.75, 128.92, 135.94, 138.18, 143.22, 152.34, 155.38, 160.10, 170.62 ppm; MS-SI (m/z) calcd. For  $\text{C}_{22}\text{H}_{24}\text{N}_2\text{O}_4$ : 380.43; found: 381.18 [ $\text{H}^+$ ]. For  $^1\text{H}$ ,  $^{13}\text{C}$  NMR and mass spectra, see [Figures S4-S6](#).



AV-400-20220407-101410-44576.001.001.1R.ESP

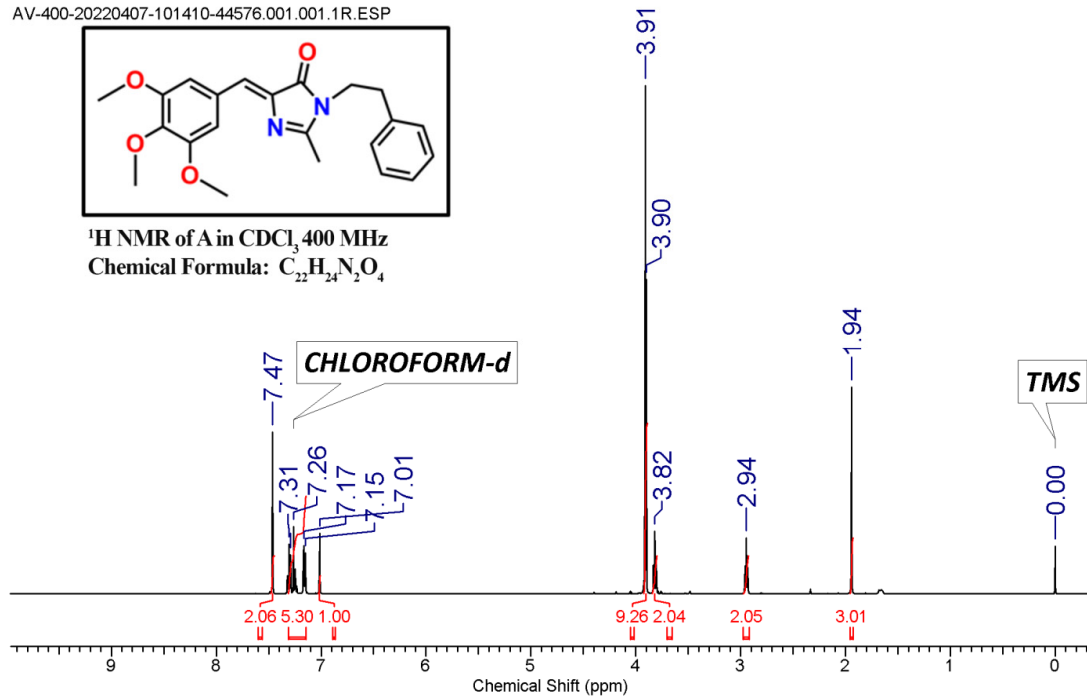


**Figure S1.** <sup>1</sup>H NMR spectrum of a compound A in CDCl<sub>3</sub>.

AV-400-20220407-101410-44576.003.001.1r.esp

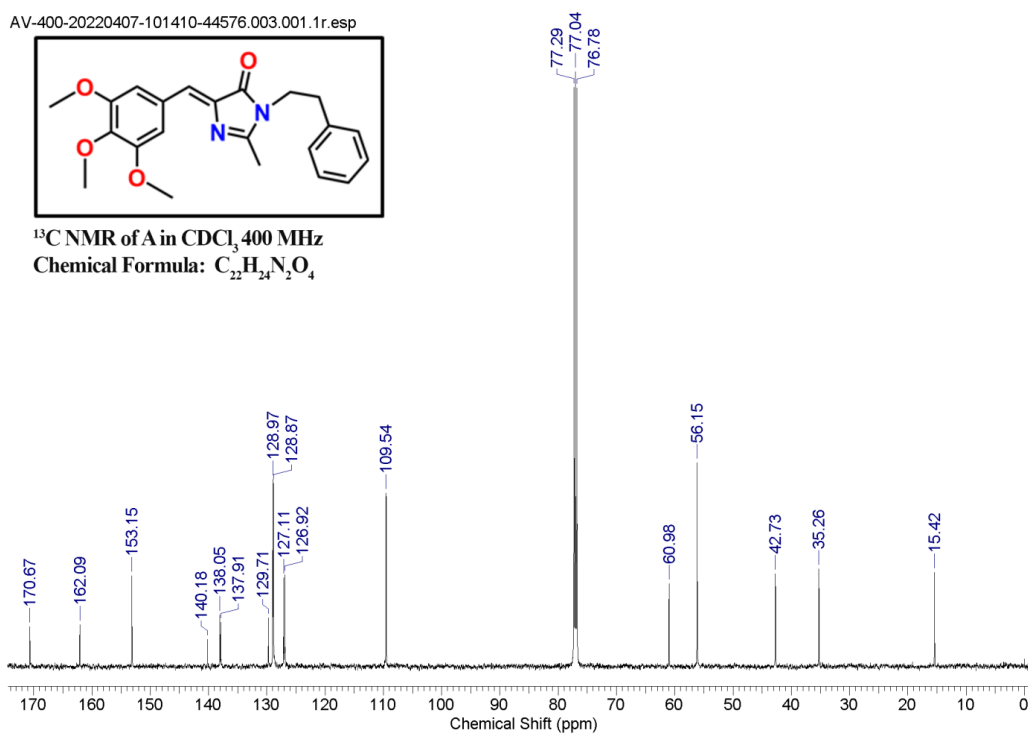


**Figure S2.** <sup>13</sup>C NMR spectrum of a compound A in CDCl<sub>3</sub>.

PA #385 RT: 1.71 AV: 1 NL: 3.36E9  
T: FTMS + p ESI Full ms [100.0000-1500.0000]

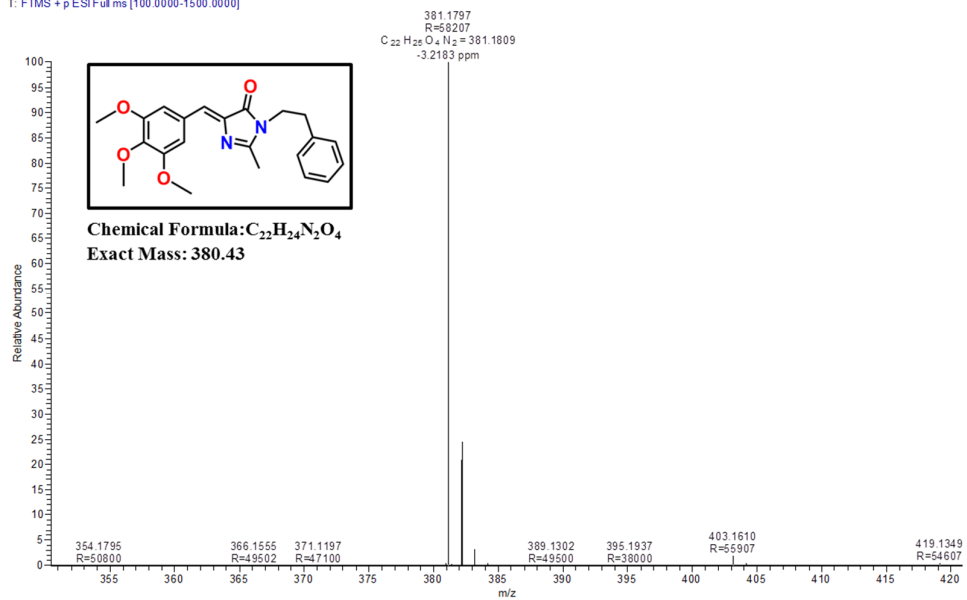
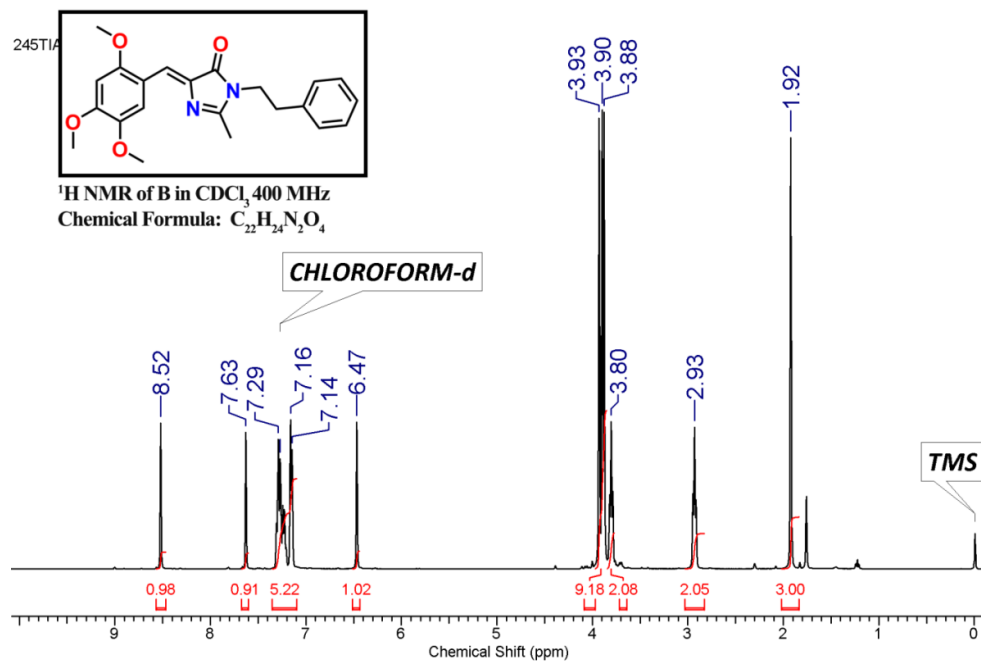


Figure S3. Mass spectrum of a compound A.



**Figure S4.** <sup>1</sup>H NMR spectrum of a compound **B** in CDCl<sub>3</sub>.

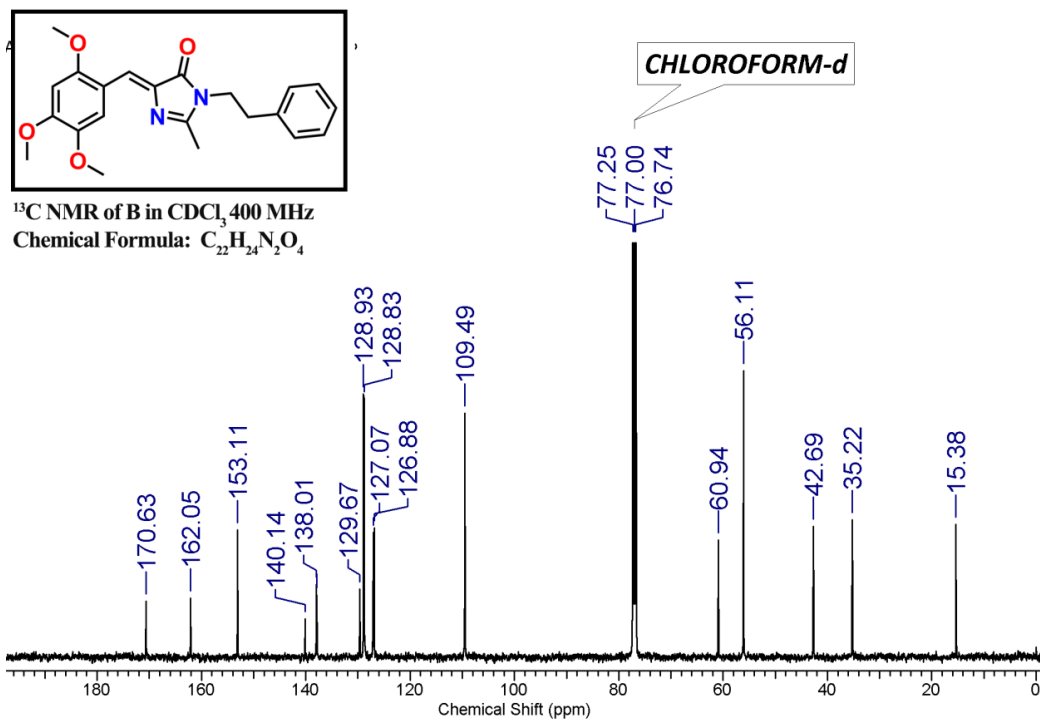
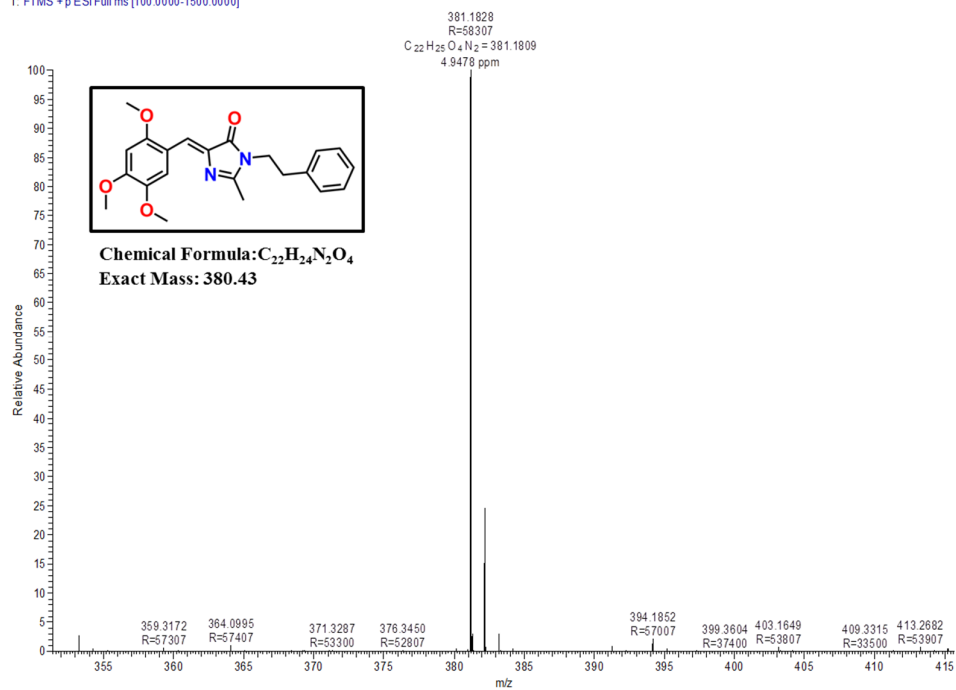


Figure S5. <sup>13</sup>C NMR spectrum of a compound **B** in CDCl<sub>3</sub>.

245-TIA-PA #577 RT: 2.57 AV: 1 NL: 1.62E8  
T: FTMS + p ESI Full ms [100.0000-1500.0000]



**Figure S6.** Mass spectrum of a compound **B**.

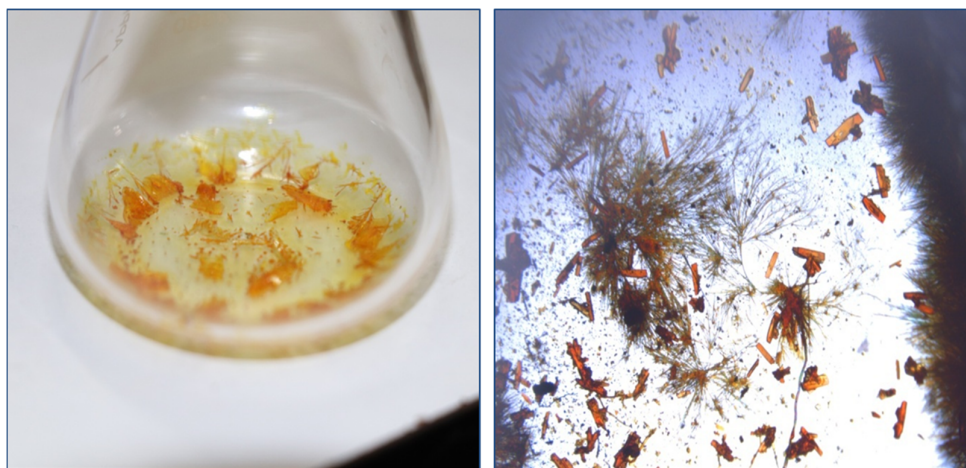
**Table S1.** Crystallization of compound **A** polymorphs from various common organic solvents by slow evaporation method.

<b>Sr. No</b>	<b>Solvent</b>	<b>Crystal Type</b>	<b>Observation</b>
1.	Methanol	Needle	Form <b>A2</b>
2.	Ethanol	Concomitant	Form <b>A1, A2</b>
3.	Acetonitrile	Needle	Form <b>A2</b>
4.	Acetone	Concomitant	Form <b>A1, A2</b>
5.	2-Propanol	Plate	Form <b>A1</b>
6.	Toluene	Plate	Form <b>A1</b>
7.	Chloroform + Methanol	Concomitant	Form <b>A1, A2</b>
8.	Acetone + Ethanol	Plate	Form <b>A1</b>
9.	Methanol + Acetonitrile	Needle	Form <b>A2</b>
10.	2-Propanol + 1-Butanol	Plate	Form <b>A1</b>

**Table S2.** Crystallization of compound **B** polymorphs from various common organic solvents by slow evaporation method.

<b>Sr. No.</b>	<b>Solvent</b>	<b>Crystal Type</b>	<b>Observation</b>
1.	Methanol	Concomitant	Form <b>B1</b> , <b>B2</b>
2.	Ethanol	Plate	Form <b>B2</b>
3.	Acetone	Concomitant	Form <b>B1</b> , <b>B2</b>
4.	1-Butanol	Plate	Form <b>B2</b>
5.	2-Propanol	Concomitant	Form <b>B1</b> , <b>B2</b>
6.	Toluene	Plate	Form <b>B2</b>
7.	Acetonitrile	Plate	Form <b>B2</b>
8.	Ethanol + Methanol	Plate	Form <b>B2</b>
9.	Ethanol + DCM	Plate	Form <b>B2</b>
10.	2-Propanol + DCM	Needle	Form <b>B1</b>
11.	Methanol + Acetonitrile	Plate	Form <b>B2</b>
12.	Acetone + 2-Propanol	Concomitant	Form <b>B1</b> , <b>B2</b>
13.	Methanol + DCM	Plate	Form <b>B2</b>





(a)

(b)

**Figure S7.** Photomicrograph of crystals of polymorphs of **A** and **B** obtained concomitantly, (a) Form **A1** (plates) and Form **A2** (needles), (b) Form **B1** (needles) and Form **B2** (plates).

**Table S3.** Single crystal X-ray diffraction data for polymorphs of compound **A** and **B**.

Crystal Data	Form A1	Form A2	Form B1	Form B2
Formula	C <sub>22</sub> H <sub>24</sub> N <sub>2</sub> O <sub>4</sub>	C <sub>22</sub> H <sub>24</sub> N <sub>2</sub> O <sub>4</sub>	C <sub>22</sub> H <sub>24</sub> N <sub>2</sub> O <sub>4</sub>	C <sub>22</sub> H <sub>24</sub> N <sub>2</sub> O <sub>4</sub>
Molecular Weight	380.43	380.43	380.43	380.43
Crystal Size, mm	0.130 x 0.120 x 0.070	0.09 x 0.08 x 0.08	0.140 x 0.110 x 0.090	0.140 x 0.110 x 0.100
Temp. (K)	100(2)	100(2)	100(2)	100(2)
Crystal Syst.	Triclinic	Monoclinic	Monoclinic	Triclinic
Space Group	P-1	P21/c	Pn	P-1
<i>a</i> /Å	6.7861(6)	7.4983(6)	5.0121(7)	7.1543(5)
<i>b</i> /Å	10.5591(9)	25.712(2)	15.791(2)	9.0388(6)
<i>c</i> /Å	14.6794(14)	10.1462(9)	12.3050(18)	15.8533(11)
$\alpha$ /°	103.839(3)	90	90	104.611(2)
$\beta$ /°	100.553(3)	96.934(3)	101.364(4)	95.711(3)
$\gamma$ /°	99.593(3)	90	90	96.882(3)
V/Å <sup>3</sup>	979.34(15)	1941.9(3)	954.8(2)	975.85(12)
Z	2	4	2	2
Radiation type	Mo K $\alpha$	Mo K $\alpha$	Mo K $\alpha$	Mo K $\alpha$
Wavelength/Å	0.71073	0.71073	0.71073	0.71073
D <sub>calc</sub> /g cm <sup>-3</sup>	1.290	1.301	1.323	1.295
m/mm <sup>-1</sup>	0.089	0.090	0.092	0.090
F(000)	404	808	404	404
Ab. Correct.	Multi-scan	Multi-scan	Multi-scan	Multi-scan
T <sub>min</sub> /T <sub>max</sub>	0.988/0.994	0.990/0.999	0.987/0.992	0.988/0.991
2 $\theta$ <sub>max</sub>	59.35	57.44	49.40	52.86
Total reflections	39408	54784	21073	23110
unique reflections	5536	5003	3161	4000
Obs. reflections	3882	4468	2100	3156
h, k, l (min, max)	(-9,9), (-13,14), (-20,19)	(-10,9), (-34,34), (-13,13)	(-5,5), (-18,18), (-14,14)	(-8,8), (-11,11), (-19,19)
R <sub>int</sub> /R <sub>sig</sub>	0.0972/0.0639	0.0659/0.0268	0.1389/0.1026	0.0728/0.0528
No. of para	257	257	258	257
R1 [I > 2 $\sigma$ (I)]	0.0670	0.0460	0.0532	0.0744
wR2 [I > 2 $\sigma$ (I)]	0.1485	0.1089	0.1012	0.1629
R1 [all data]	0.1036	0.0522	0.1102	0.0975
wR2 [all data]	0.1649	0.1124	0.1252	0.1732
Goodness-of-fit (S)	1.063	1.101	1.006	1.165
$\Delta\rho_{max}$ , $\Delta\rho_{min}$ (eÅ <sup>-3</sup> )	0.556, -0.324	0.302, -0.227	0.215, -0.231	0.278, -0.242
CCDC nos.	2298736	2298737	2298738	2298739

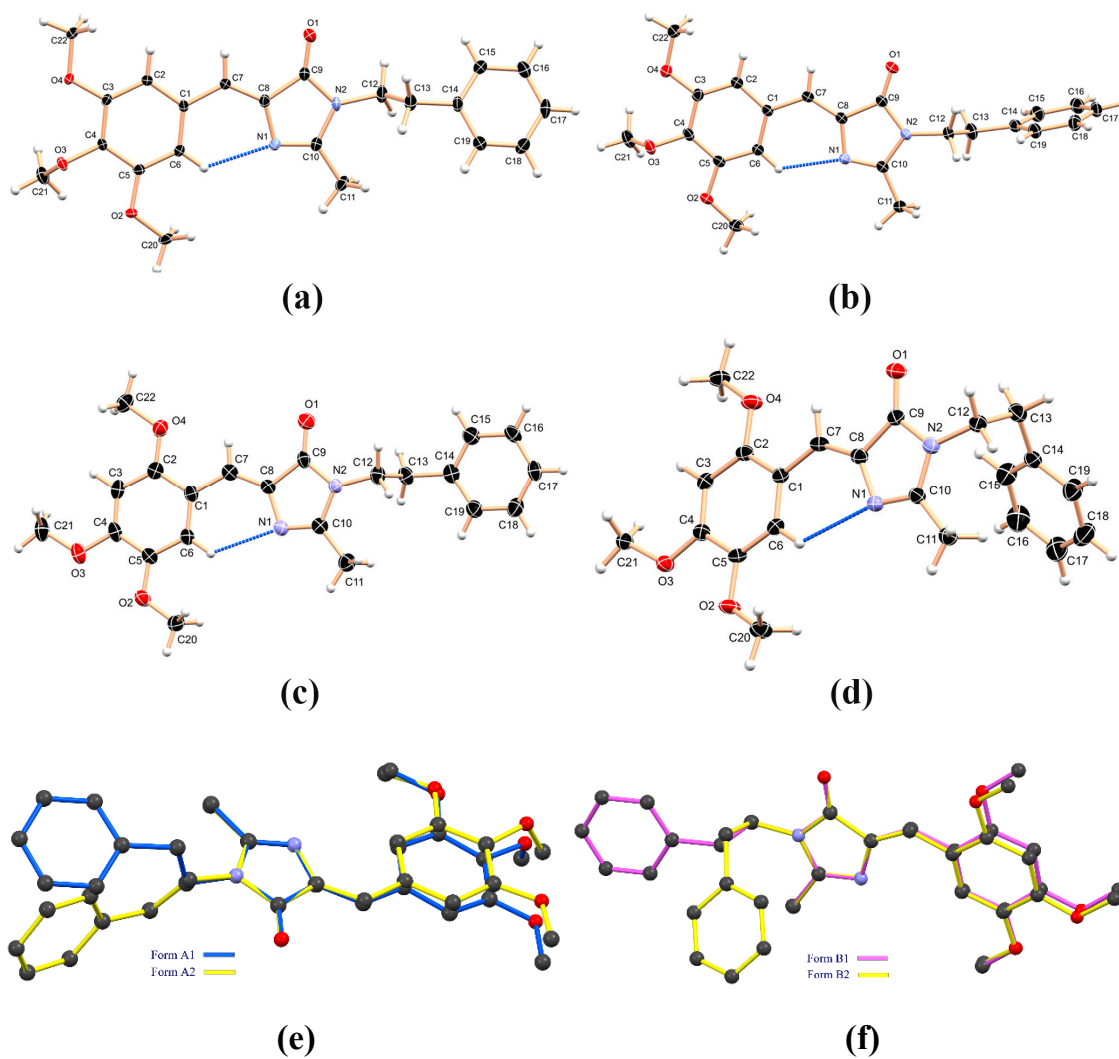


**Figure S8.** The Oak Ridge Thermal Ellipsoid Plots (ORTEPs) of (a) Form A1, (b) Form A2, (c) Form B1 and (d) Form B2 drawn at the 50% ellipsoid probability level and hydrogen atoms are displayed as small spheres with radii 0.07 Å and (e) and (f) are the structure overlay of polymorphs (Forms A1 & A2 and Forms B1 & B2) of compounds A and B, respectively.

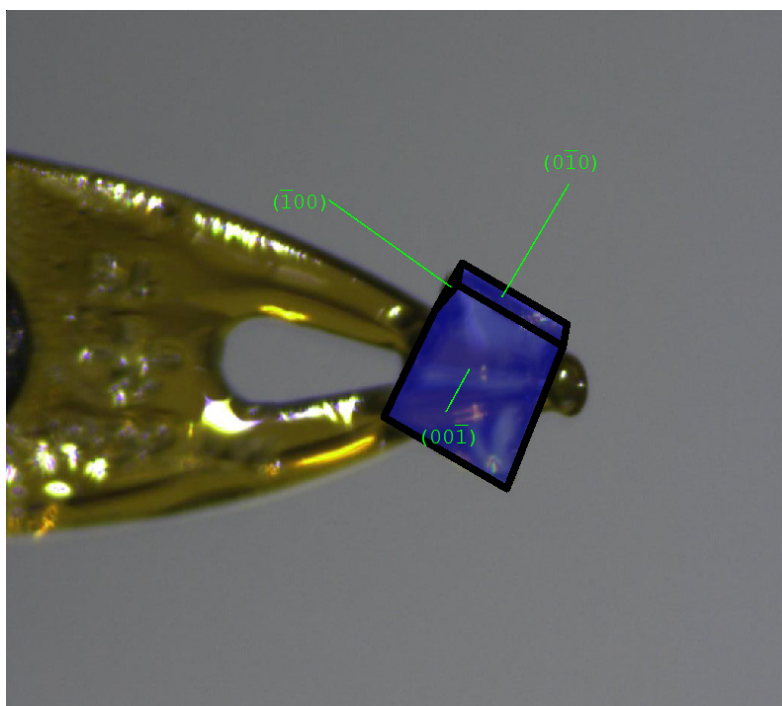


**Figure S9.** Face indices image of Form A1 crystal.

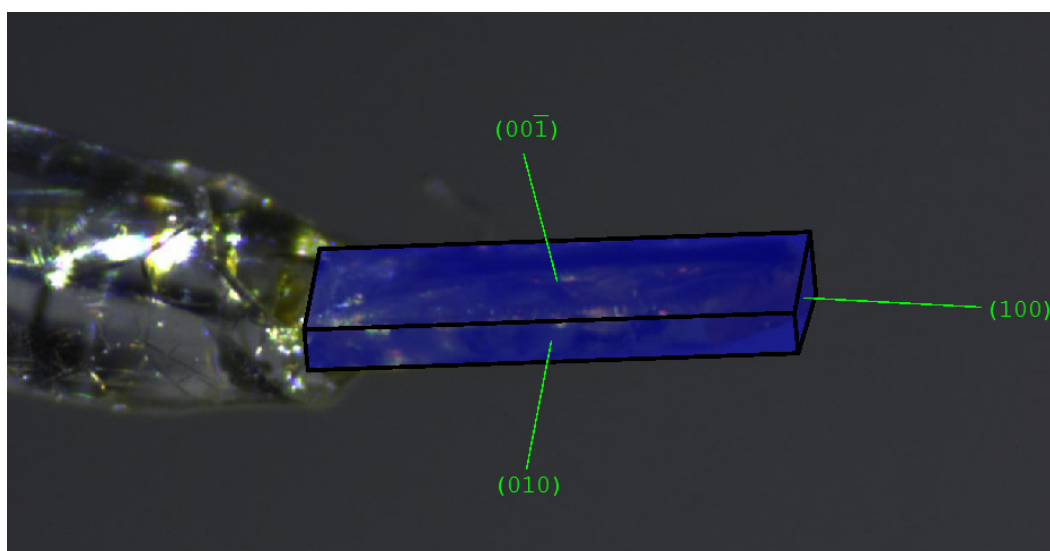


**Figure S10.** Face indices image of Form A2 crystal.

**Table S4.** Geometrical parameters of intermolecular interactions in all the polymorphs of A.

Sr. No.	D-H...A	D-H (Å)	H...A (Å)	D...A/ Cg...Cg (Å)	D-H...A / $\alpha$ (°)	Symmetry Codes
<b>Form A1</b>						
1.	C6-H6...N1	0.95	2.33	3.000(2)	127	$x, y, z$
2.	C2-H2...O1	0.95	2.56	3.504(3)	175	$2-x, 2-y, 1-z$
3.	C17-H17...O4	0.95	2.57	3.393(3)	145	$-2+x, y, -1+z$
4.	C20-H20B...O4	0.98	2.70	3.669(3)	168	$-1+x, y, z$
5.	C13-H13B...O2	0.99	2.64	3.481(2)	143	$1-x, 1-y, 1-z$
6.	C19-H19...O3	0.95	2.64	3.518(3)	155	$1-x, 1-y, 1-z$
7.	C20-H20A...Cg1	0.98	2.89	3.426(2)	116	$1-x, 1-y, 1-z$
8.	C21-H21A...Cg3	0.98	2.96	3.392(2)	108	$1+x, y, 1+z$
9.	C9=O1...Cg1			3.2476(18)	99.28(13)	$1-x, 2-y, 1-z$
10.	Cg1...Cg1	-	-	4.3791(13)	0.00(11)	$1-x, 2-y, 1-z$
<b>Form A2</b>						
1.	C6-H6...N1	0.95	2.30	2.9658(16)	127	$x, y, z$
2.	C2-H2...O1	0.95	2.66	3.5217(15)	151	$1-x, 1-y, 1-z$
3.	C7-H7...O1	0.95	2.59	3.4820(15)	157	$1-x, 1-y, 1-z$
4.	C11-H11C...O3	0.98	2.41	3.2423(16)	143	$-1+x, 3/2-y, -1/2+z$
5.	C12-H12B...O2	0.99	2.59	3.3876(16)	138	$-x, 1-y, 1-z$
6.	C17-H17...O1	0.95	2.67	3.380(2)	132	$-x, -1/2+y, 1/2-z$
7.	C21-H21B...O4	0.98	2.71	3.506(2)	139	$x, 3/2-y, -1/2+z$
8.	C11-H11A...Cg2	0.98	2.68	3.4381(14)	134	$-1+x, y, z$
9.	C15-H15...Cg1	0.95	2.88	3.6889(15)	143	$-x, 1-y, -z$
10.	C20-H20A...Cg2	0.98	2.89	3.5066(15)	122	$x, 3/2-y, -1/2+z$
11.	C22-H22A...Cg3	0.98	2.63	3.3946(16)	135	$1-x, 1-y, 1-z$
12.	Cg1...Cg2	-	-	4.3115(8)	6.74(6)	$-1+x, y, z$
13.	Cg3...Cg3	-	-	4.3257(9)	0.03(7)	$-1-x, 1-y, -z$
D-H = Donor- Hydrogen bond length in Angstrom (Å), H...A = Hydrogen...Acceptor bond length in Angstrom (Å), D...A = Donor...Acceptor bond length in Angstrom (Å), D-H...A = bond angle in degrees (°), Cg...Cg = distance between ring Centroids in Angstrom (Å), $\alpha$ = dihedral angle between planes of two aromatic rings in degrees (°), For polymorphs Form A1 and Form A2; Cg1: N1/C8/C9/N2/C10; Cg2: C1-C6; Cg3: C14-C19.						

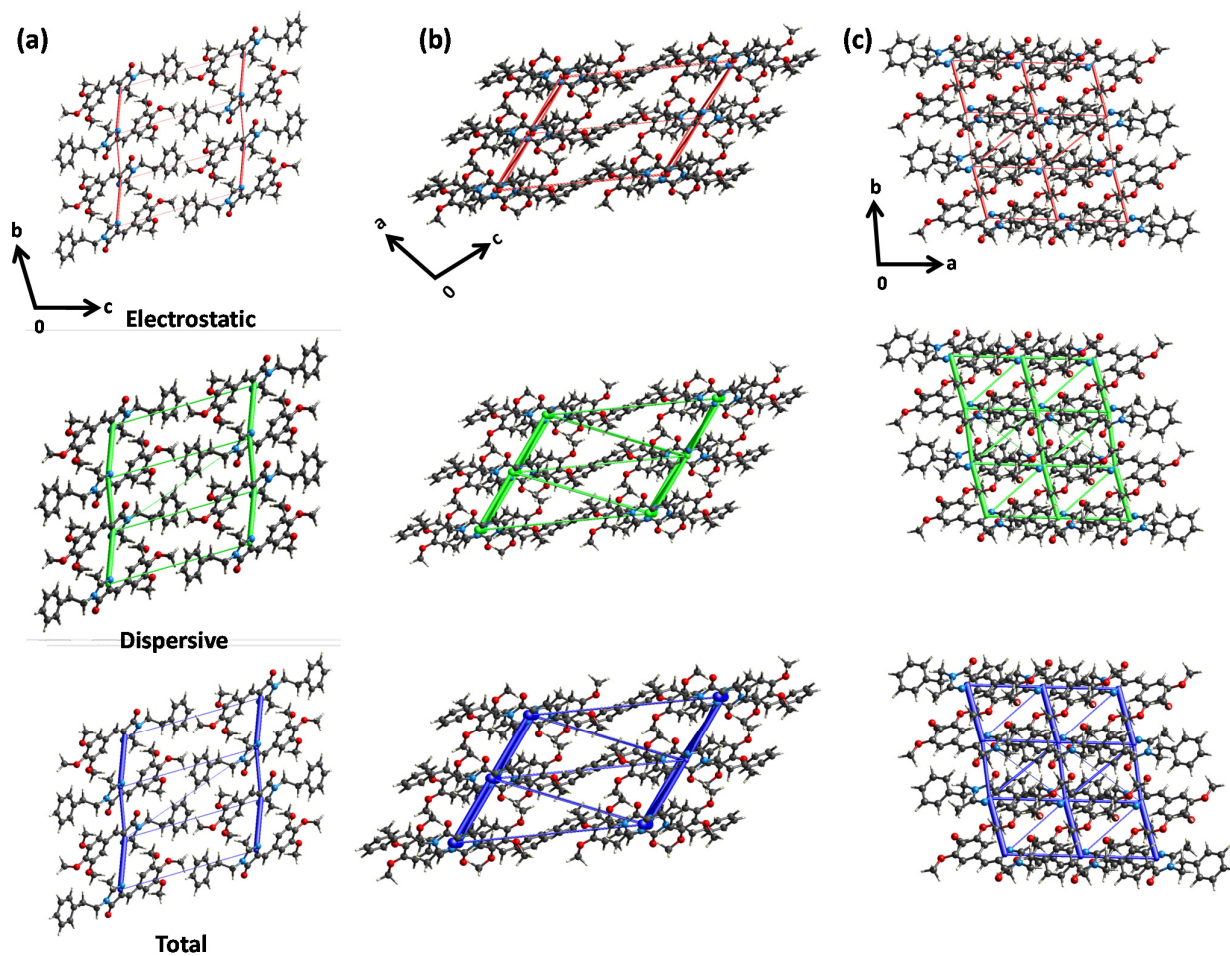
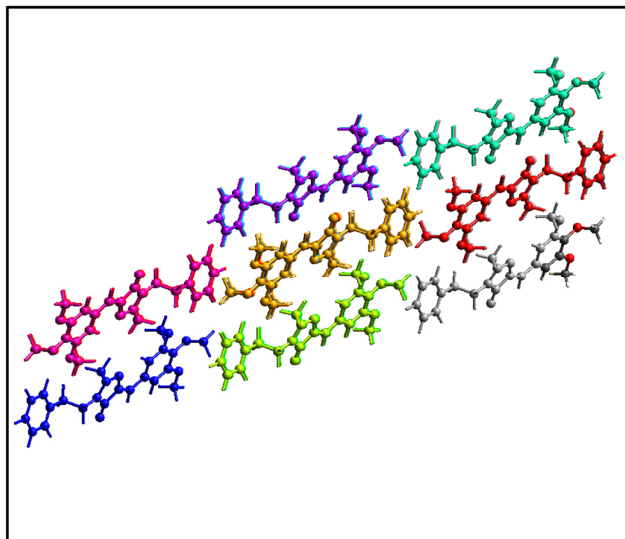


**Figure S11.** Visualization of energy frameworks showing electrostatic (red), dispersion (green) components and total interaction energy (blue) for Form A1, in the (a) (100), (b) (010) and (c) (001) faces, respectively. The energy threshold is  $5 \text{ kJ mol}^{-1}$ .

**Table S5.** Interaction energy based on energy frameworks for Form A1 crystals.



Interaction Energies (kJ/mol)  
R is the distance between molecular centroids (mean atomic position) in Å.

Total energies, only reported for two benchmarked energy models, are the sum of the four energy components, scaled appropriately (see the scale factor table below)

	N	Symop	R	Electron Density	E_ele	E_pol	E_dis	E_rep	E_tot
	2	X, Y, Z	15.00	B3LYP/6-31G(d,p)	-3.3	-0.4	-20.3	14.4	-12.6
	2	X, Y, Z	6.79	B3LYP/6-31G(d,p)	-16.0	-3.9	-47.9	27.8	-44.4
	1	-X, -Y, -Z	5.24	B3LYP/6-31G(d,p)	-44.4	-11.6	-98.2	73.7	-95.4
	1	-X, -Y, -Z	8.05	B3LYP/6-31G(d,p)	-0.8	-1.2	-32.4	19.5	-17.9
	1	-X, -Y, -Z	17.27	B3LYP/6-31G(d,p)	-2.1	-0.2	-8.1	3.1	-7.5
	1	-X, -Y, -Z	5.34	B3LYP/6-31G(d,p)	-13.0	-4.6	-82.1	40.2	-50.9
	1	-X, -Y, -Z	17.49	B3LYP/6-31G(d,p)	-1.5	-0.1	-4.3	2.3	-4.1
	1	-X, -Y, -Z	7.71	B3LYP/6-31G(d,p)	-20.7	-11.4	-38.4	42.2	-37.7
	1	X, Y, Z	18.08	B3LYP/6-31G(d,p)	-5.3	-1.7	-15.0	12.4	-12.3

Scale factors for benchmarked energy models  
See Mackenzie et al. IUCrJ (2017)

Energy Model	k_ele	k_pol	k_disp	k_rep
CE+HF ... HF/3-21G electron densities	1.019	0.651	0.901	0.811
CE-B3LYP ... B3LYP/6-31G(d,p) electron densities	1.057	0.740	0.871	0.618



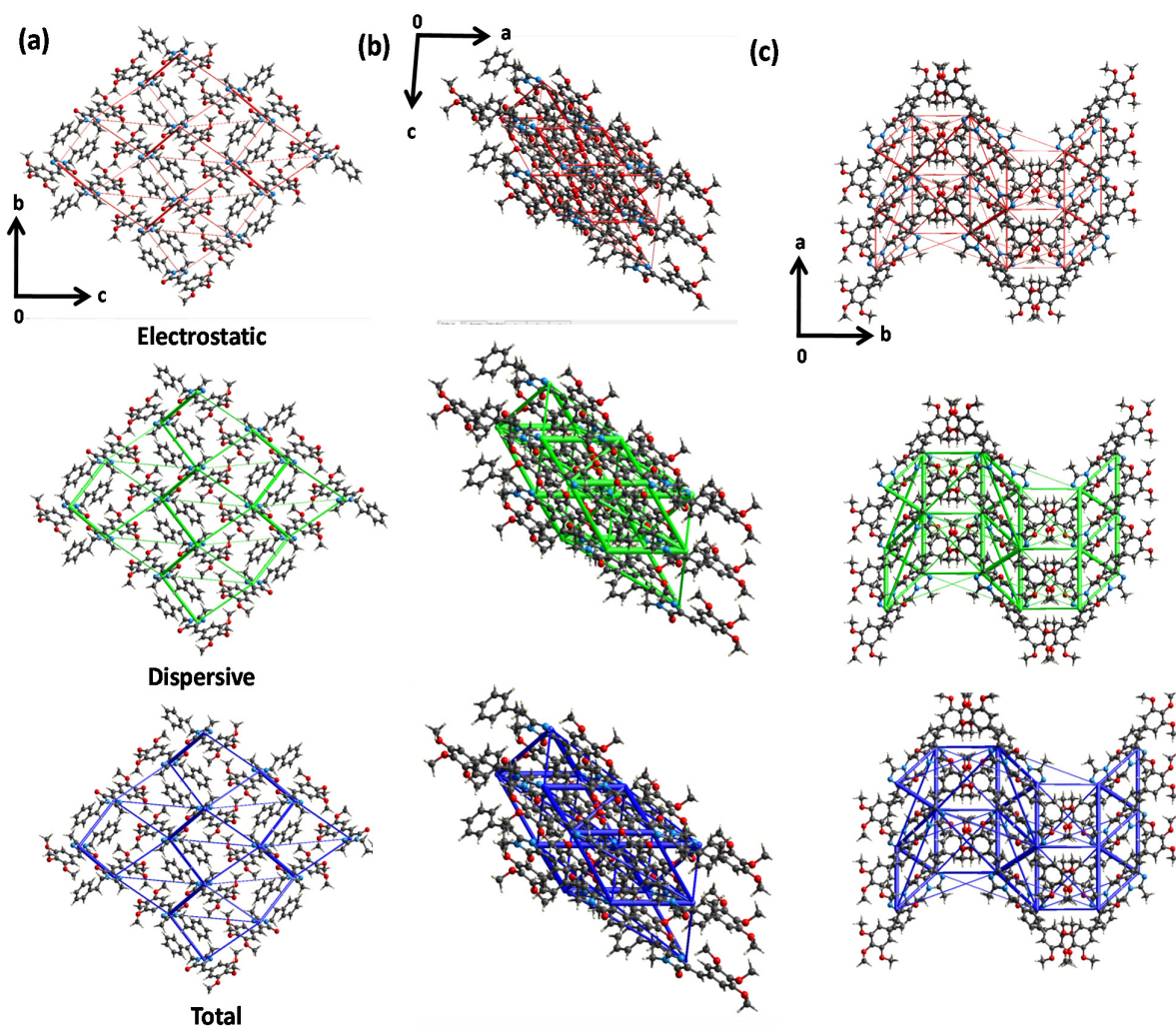
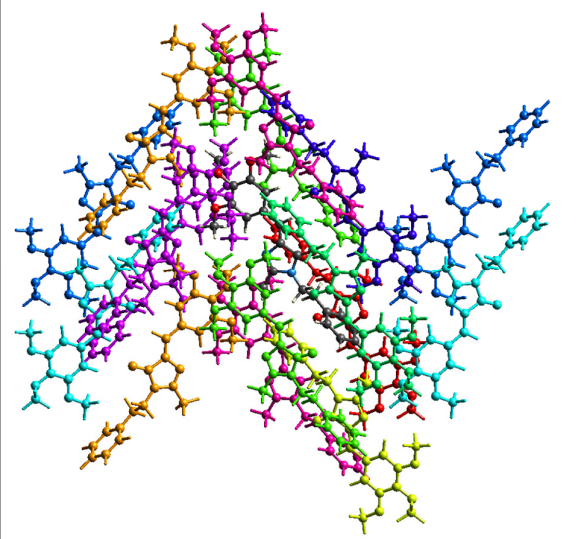


**Figure S12.** Visualization of energy frameworks showing electrostatic (red), dispersion (green) components and total interaction energy (blue) for Form A2, in the (a) (100), (b) (010) and (c) (001) faces, respectively. The energy threshold is  $5 \text{ kJ mol}^{-1}$ .



**Table S6.** Interaction energy based on energy frameworks for Form A2 crystals.



Interaction Energies (kJ/mol)  
R is the distance between molecular centroids (mean atomic position) in Å.

Total energies, only reported for two benchmarked energy models, are the sum of the four energy components, scaled appropriately (see the scale factor table below)

N	Symp	R	Electron Density	E_ele	E_pol	E_dis	E_rep	E_tot
1	-x, -y, -z	9.21	B3LYP/6-31G(d,p)	-8.2	-2.7	-52.4	29.0	-38.5
2	x, -y+1/2, z+1/2	11.49	B3LYP/6-31G(d,p)	-10.6	-3.0	-15.7	12.4	-19.5
1	-x, -y, -z	14.19	B3LYP/6-31G(d,p)	-5.5	-2.1	-38.6	27.3	-24.1
2	x, y, z	7.50	B3LYP/6-31G(d,p)	-18.7	-5.0	-73.2	49.5	-56.6
1	-x, -y, -z	8.18	B3LYP/6-31G(d,p)	-14.0	-5.8	-40.3	25.5	-38.5
2	-x, y+1/2, -z+1/2	13.74	B3LYP/6-31G(d,p)	-6.4	-1.5	-10.4	6.4	-12.9
2	-x, y+1/2, -z+1/2	13.25	B3LYP/6-31G(d,p)	-1.5	-0.3	-4.5	1.4	-4.8
1	-x, -y, -z	6.66	B3LYP/6-31G(d,p)	-29.2	-9.6	-57.2	53.6	-54.6
2	x, -y+1/2, z+1/2	9.22	B3LYP/6-31G(d,p)	-5.6	-2.1	-26.5	14.7	-21.4
2	x, y, z	11.87	B3LYP/6-31G(d,p)	-0.2	-0.2	-2.6	0.0	-2.7

Scale factors for benchmarked energy models  
See Mackenzie et al. IUCr (2017)

Energy Model	k_ele	k_pol	k_dis	k_rep
CE+HF ... HF/3-21G electron densities	1.019	0.651	0.901	0.811
CE-B3LYP ... B3LYP/6-31G(d,p) electron densities	1.057	0.740	0.871	0.618

**Table S7.** Geometrical parameters of intermolecular interactions in all the polymorphs of **B**.

Sr. No.	D-H...A	D-H (Å)	H...A (Å)	D...A/Cg...Cg (Å)	D-H...A / $\alpha$ (°)	Symmetry Codes
<b>Form B1</b>						
1.	C6-H6...N1	0.95	2.44	3.101(8)	127	$x, y, z$
2.	C11-H11A...N1	0.98	2.67	3.621(8)	163	$1+x, y, z$
3.	C11-H11B...O1	0.98	2.60	3.554(8)	163	$\frac{1}{2}+x, 1-y, \frac{1}{2}+z$
4.	C19-H19...O1	0.95	2.57	3.434(7)	151	$\frac{1}{2}+x, 1-y, \frac{1}{2}+z$
5.	C20-H20C...O3	0.98	2.66	3.521(8)	146	$1+x, y, z$
6.	C12-H12A...Cg1	0.99	2.95	3.790(7)	144	$1+x, y, z$
7.	C13-H13B...Cg3	0.99	2.82	3.469(7)	123	$-1+x, y, z$
8.	C21-H21C...Cg2	0.98	2.76	3.695(7)	160	$-1+x, y, z$
9.	Cg1...Cg2	-	-	3.850(4)	3.2(3)	$1+x, y, z$
<b>Form B2</b>						
1.	C6-H6...N1	0.95	2.44	3.100(3)	126	$x, y, z$
2.	C13-H13B...O2	0.99	2.48	3.266(3)	136	$1+x, -1+y, z$
3.	C21-H21A...O1	0.98	2.39	3.298(3)	153	$-1+x, 1+y, z$
4.	C21-H21C...O1	0.98	2.60	3.427(3)	142	$1-x, 1-y, 2-z$
5.	C17-H17...N1	0.95	2.57	3.482(4)	161	$1-x, -y, 1-z$
6.	C11-H11A...Cg3	0.98	2.84	3.694(3)	147	$x, y, z$
7.	C21-H21B...Cg1	0.98	2.70	3.512(3)	141	$x, 1+y, z$
8.	Cg2...Cg2	-	-	4.6439(15)	0.00(12)	$1-x, 1-y, 2-z$
9.	Cg1...Cg3	-	-	4.3176(16)	38.94(15)	$x, y, z$
D-H = Donor- Hydrogen bond length in Angstrom (Å), H...A = Hydrogen...Acceptor bond length in Angstrom (Å), D...A = Donor...Acceptor bond length in Angstrom (Å), D-H...A = bond angle in degrees (°), Cg...Cg = distance between ring Centroids in Angstrom (Å), $\alpha$ = dihedral angle between planes of two aromatic rings in degrees (°), For polymorphs Form <b>B1</b> and Form <b>B2</b> ; Cg1: N1/C8/C9/N2/C10; Cg2: C1-C6; Cg3: C14-C19.						

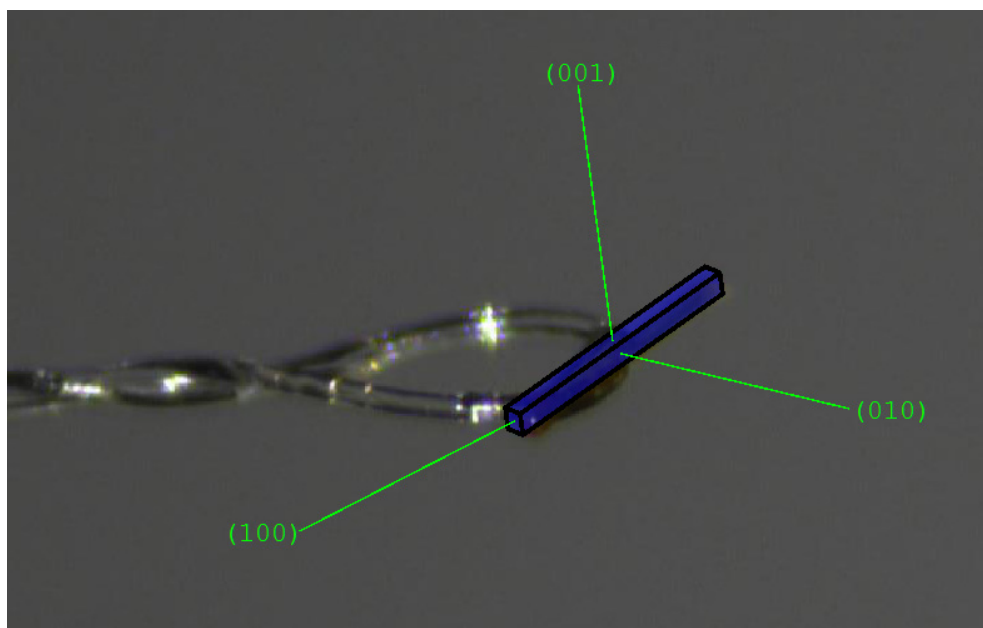


**Figure S13.** Face indices image of Form **B1** crystal.

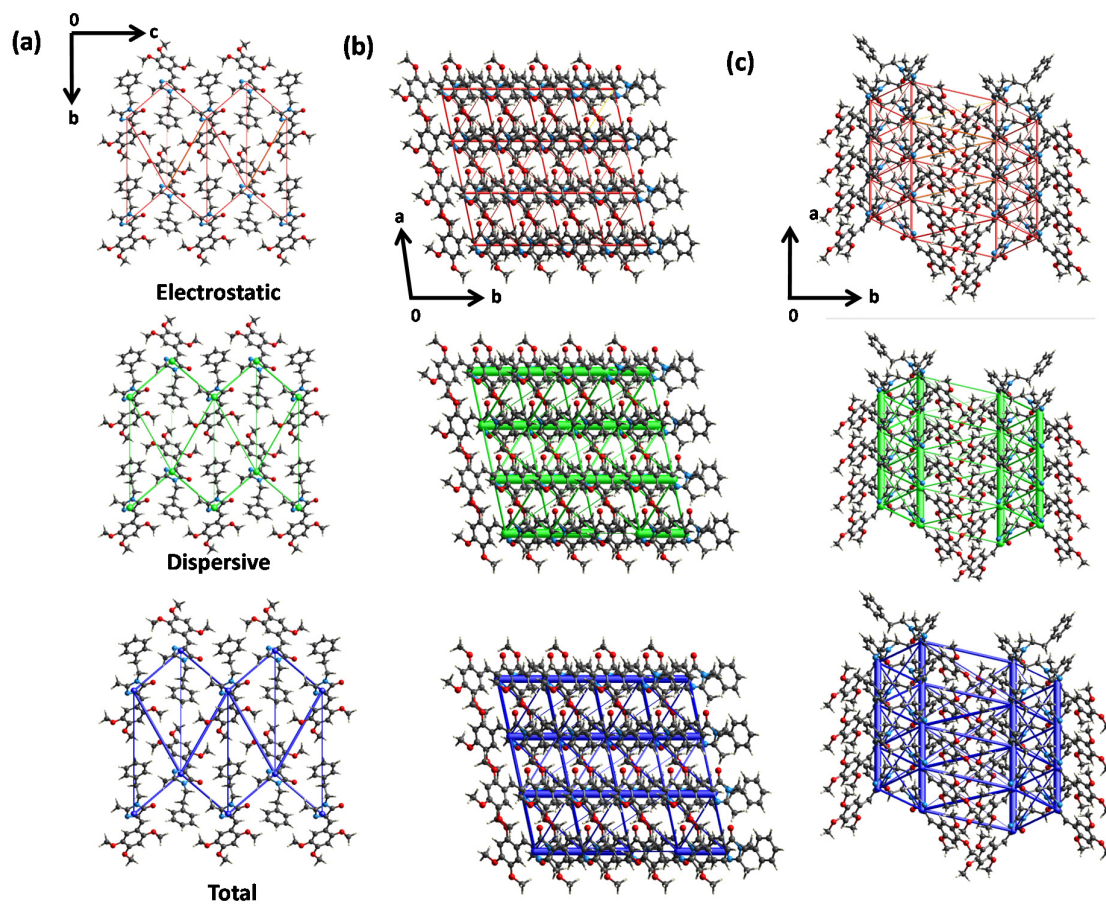


**Figure S14.** Visualization of energy frameworks showing electrostatic (red), dispersion (green) components and total interaction energy (blue) for Form **B1**, in the (a) (100), (b) (010) and (c) (001) faces, respectively. The energy threshold is  $5 \text{ kJ mol}^{-1}$ .

**Table S8.** Interaction energy based on energy frameworks for Form **B1** crystals.

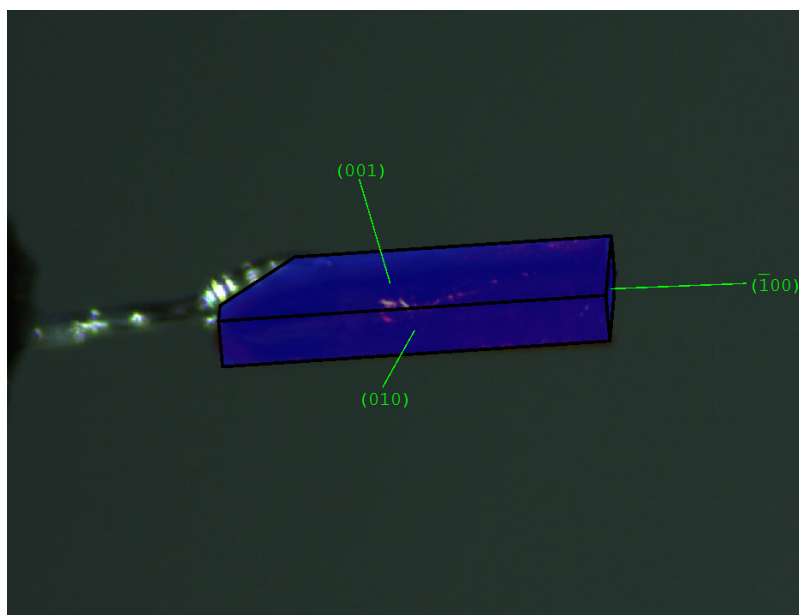
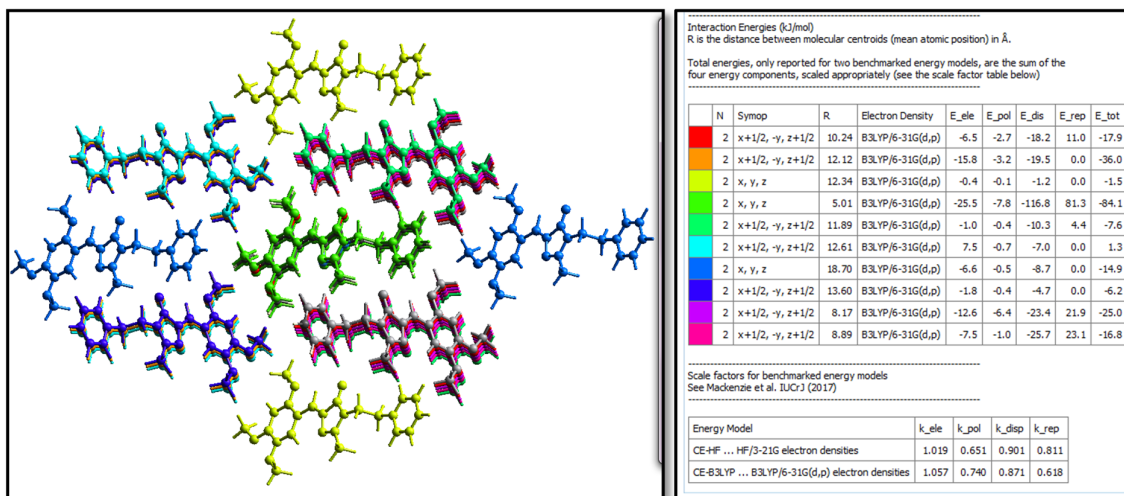


**Figure S15.** Face indices image of Form **B2** crystal.

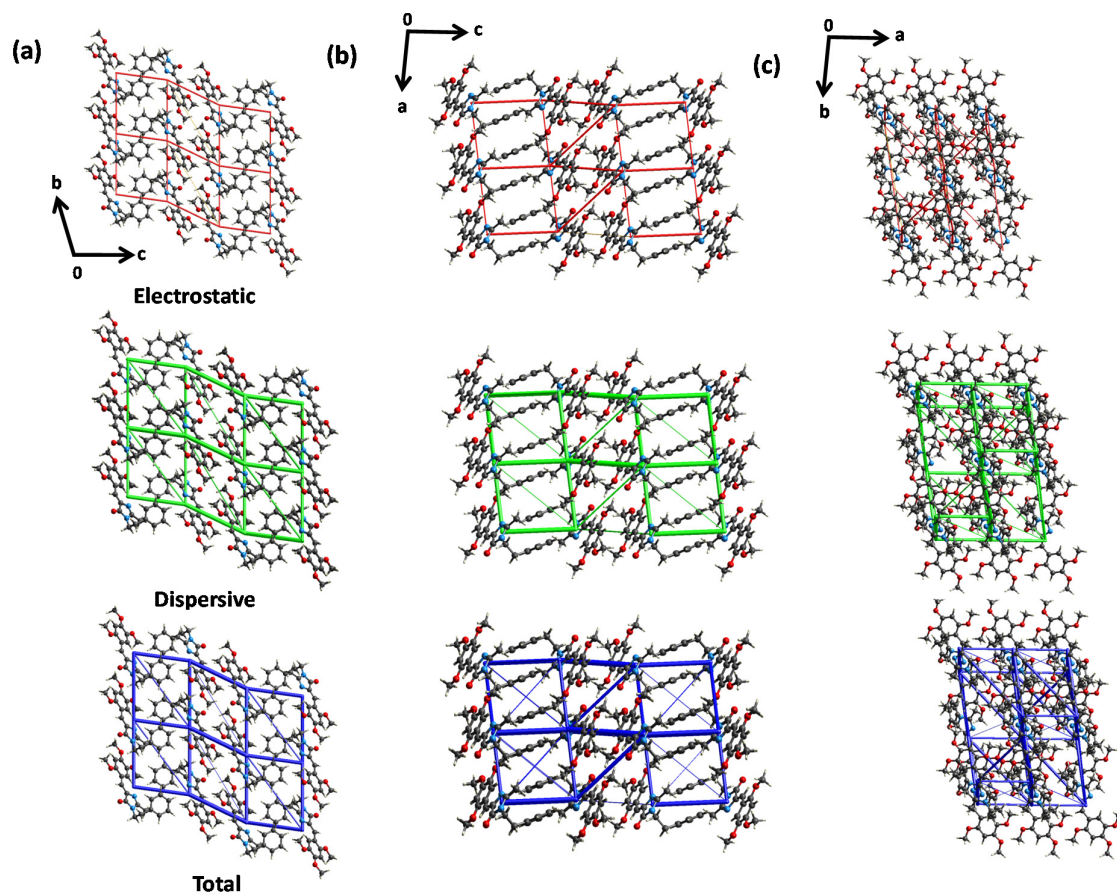
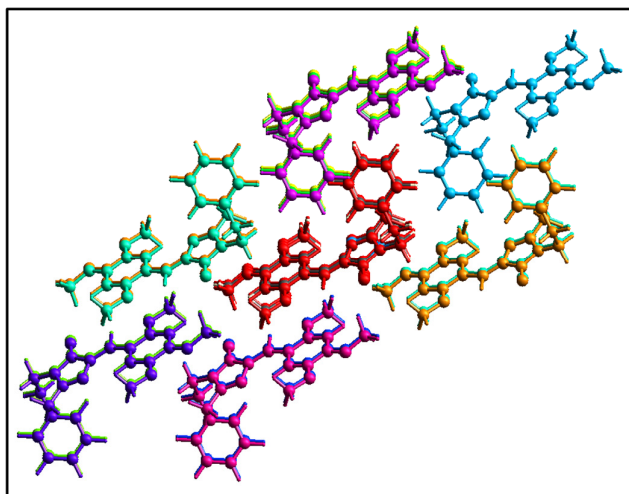


**Figure S16.** Visualization of energy frameworks showing electrostatic (red), dispersion (green) components and total interaction energy (blue) for Form **B2**, in the (a) (100), (b) (010) and (c) (001) faces, respectively. The energy threshold is  $5 \text{ kJ mol}^{-1}$ .

**Table S9.** Interaction energy based on energy frameworks for Form **B2** crystals.



Interaction Energies (kJ/mol)  
R is the distance between molecular centroids (mean atomic position) in Å.

Total energies, only reported for two benchmarked energy models, are the sum of the four energy components, scaled appropriately (see the scale factor table below)

N	Symp	R	Electron Density	E_ele	E_pol	E_dis	E_rep	E_tot
2	x, y, z	7.15	B3LYP/6-31G(d,p)	-0.5	-2.5	-47.4	27.0	-27.0
2	x, y, z	12.18	B3LYP/6-31G(d,p)	-11.5	-6.6	-20.7	0.0	-35.1
1	-x, -y, -z	10.16	B3LYP/6-31G(d,p)	-0.8	-0.1	-5.6	0.4	-5.5
1	-x, -y, -z	17.80	B3LYP/6-31G(d,p)	-1.2	-0.1	-1.3	0.0	-2.5
1	-x, -y, -z	7.92	B3LYP/6-31G(d,p)	-23.0	-4.7	-57.4	48.2	-48.0
2	x, y, z	9.04	B3LYP/6-31G(d,p)	-16.8	-3.8	-44.1	25.5	-43.3
1	-x, -y, -z	12.89	B3LYP/6-31G(d,p)	2.9	-0.7	-26.3	0.0	-20.4
1	-x, -y, -z	8.46	B3LYP/6-31G(d,p)	-21.5	-7.3	-63.4	43.0	-56.8
1	-x, -y, -z	14.92	B3LYP/6-31G(d,p)	6.8	-1.6	-16.3	0.0	-8.2
1	-x, -y, -z	11.17	B3LYP/6-31G(d,p)	-0.3	-0.3	-10.2	1.9	-8.3
1	-x, -y, -z	9.77	B3LYP/6-31G(d,p)	-19.6	-5.8	-19.3	14.9	-32.6

Scale factors for benchmarked energy models  
See Mackenzie et al. IUCrJ (2017)



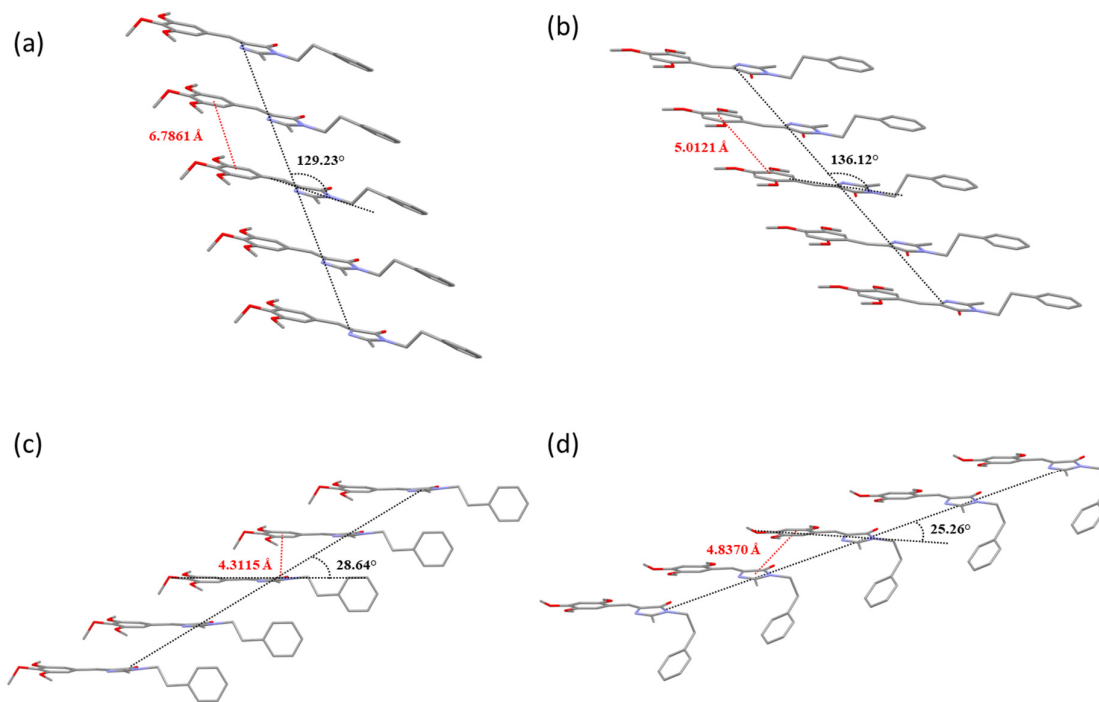


**Figure S17.** H-aggregation (head-to-head) of molecules in Form A1 (a) and Form B1 (b) and J-aggregation (head-to-tail) of molecules in Form A2 (c) and Form B2 (d).



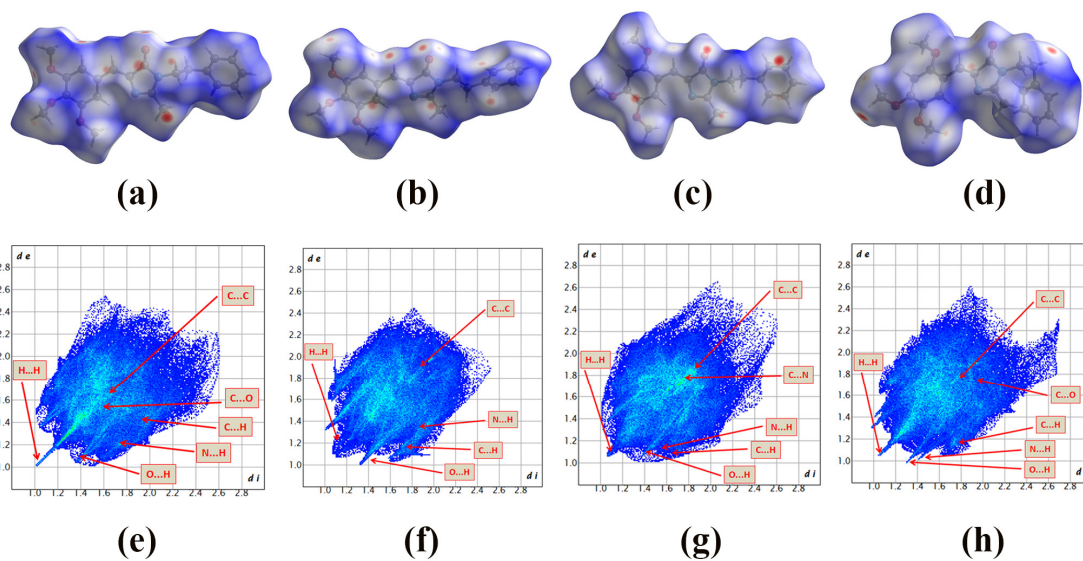


**Figure S18.** Hirshfeld surfaces for (a) Form A1, (b) Form A2, (c) Form B1 and (d) Form B2, and (e), (f), (g) and (h) are fingerprint plots of the Hirshfeld surfaces for Form A1, A2, B1 & B2 respectively.

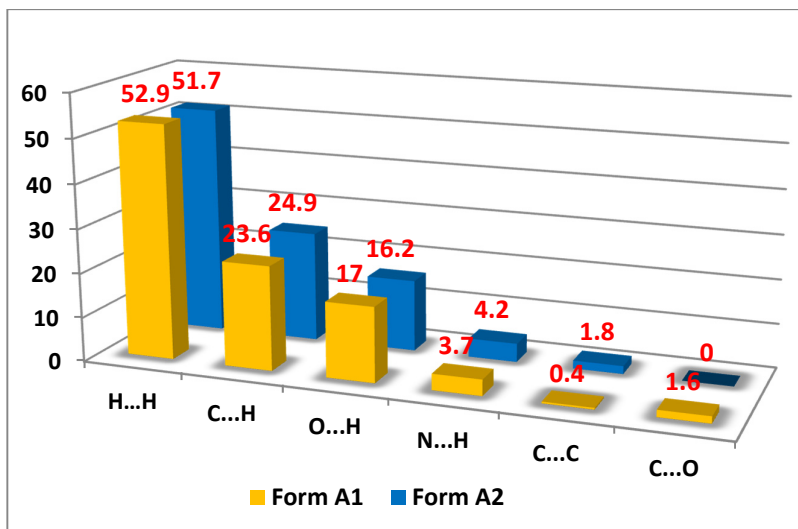


**Figure S19.** The contributions of various intermolecular interactions to Hirshfeld surfaces areas in Form A1 and Form A2 polymorphs of A.

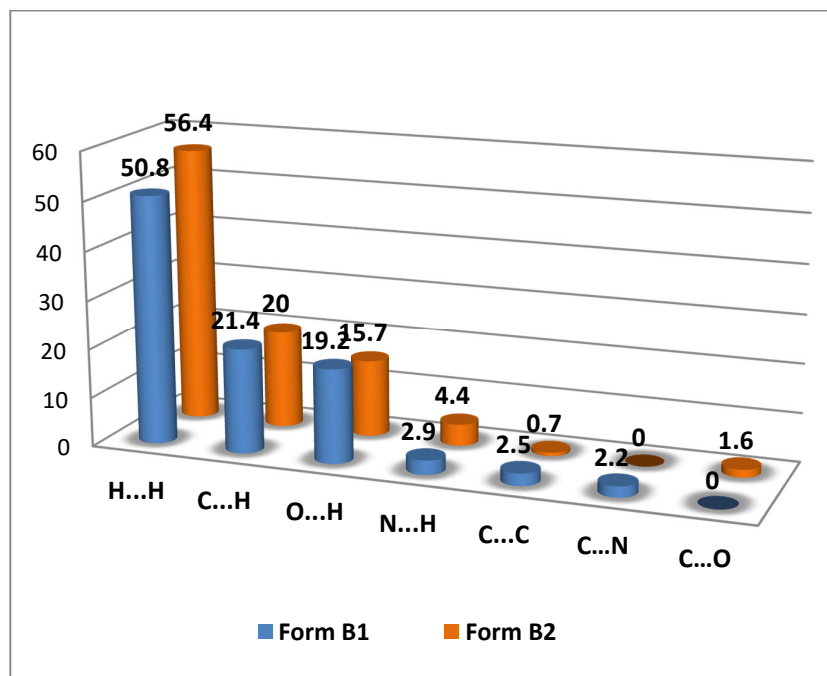


**Figure S20.** The contributions of various intermolecular interactions to Hirshfeld surfaces areas in Form **B1** and Form **B2** polymorphs of **B**.

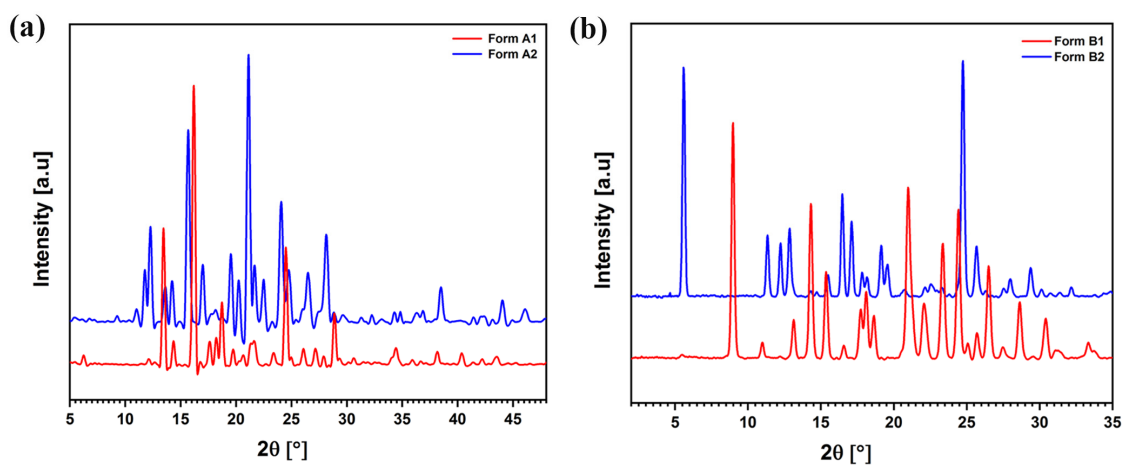


**Figure S21.** Overlay of the PXRD patterns of the polymorphs of (a) compound **A** and (b) compound **B**.

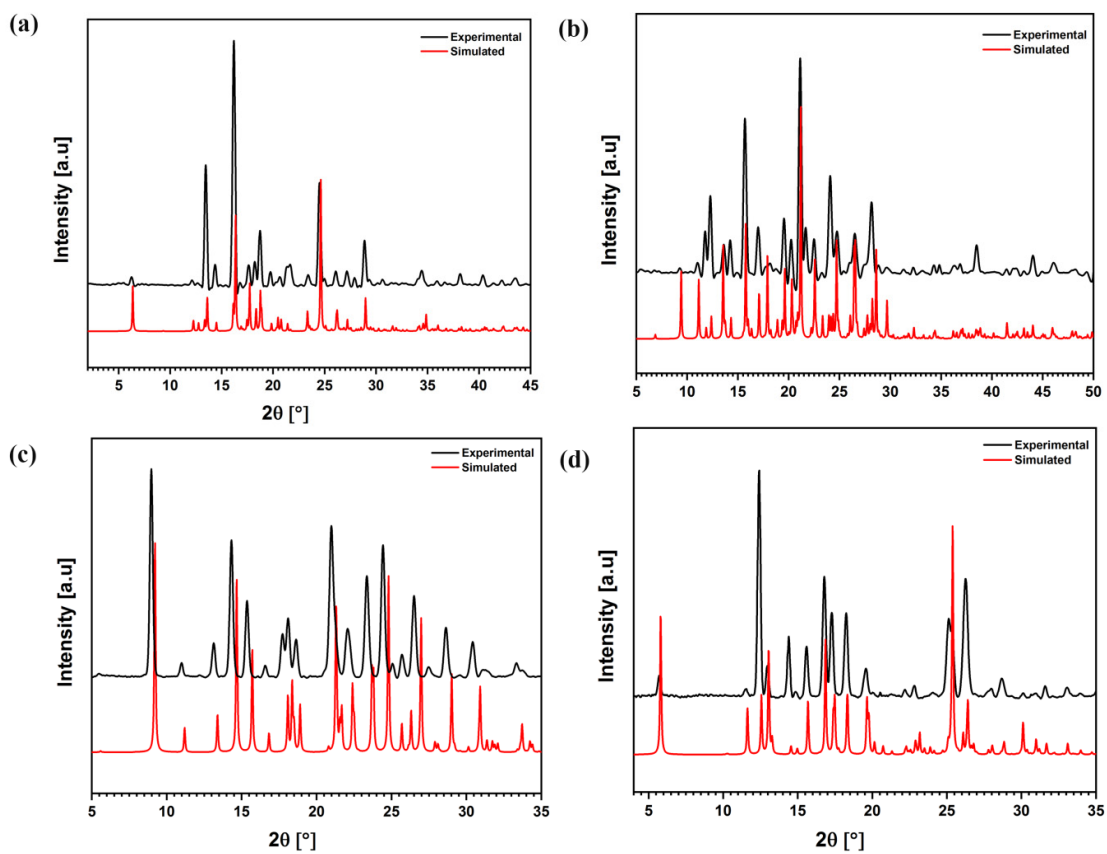


**Figure S22.** Overlay of experimental (black) and calculated (red) powder X-ray diffraction patterns of (a) Form A1, (b) Form A2, (c) Form B1 and (d) Form B2 crystals.

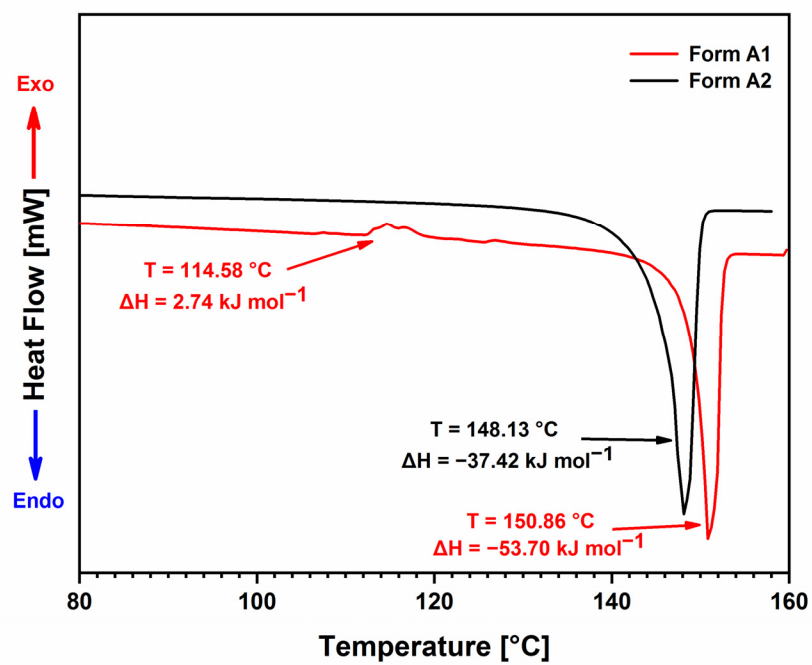


Figure S23. DSC thermograms for all the polymorphs of A.

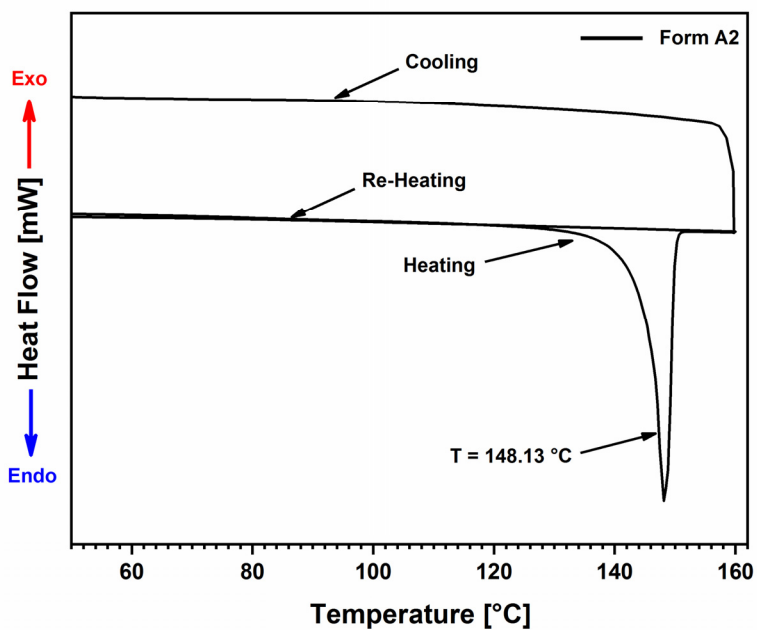


Figure S24. DSC thermogram of Form A2 crystals.

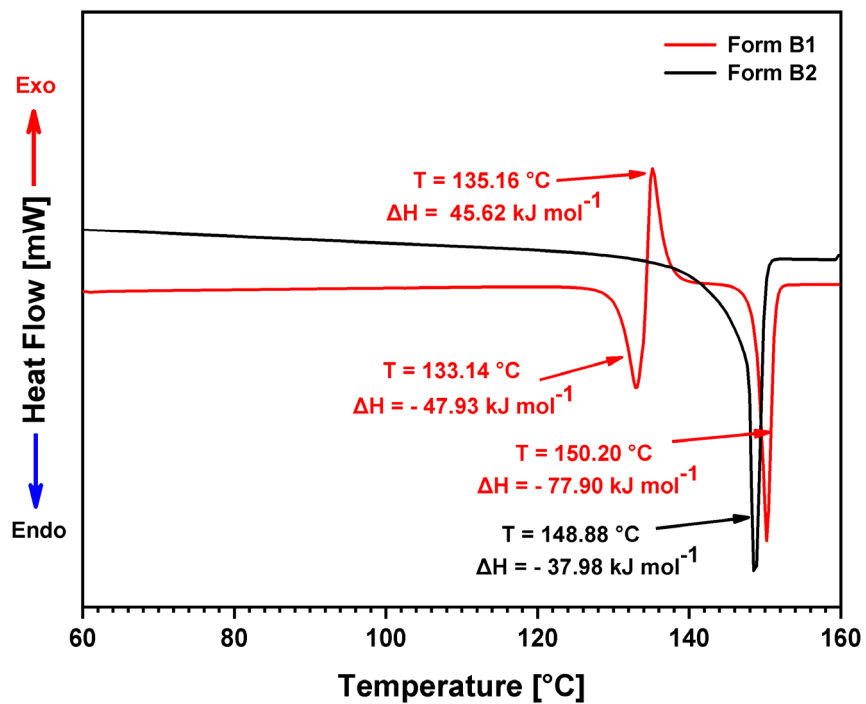


Figure S25. DSC thermograms for all the polymorphs of B.

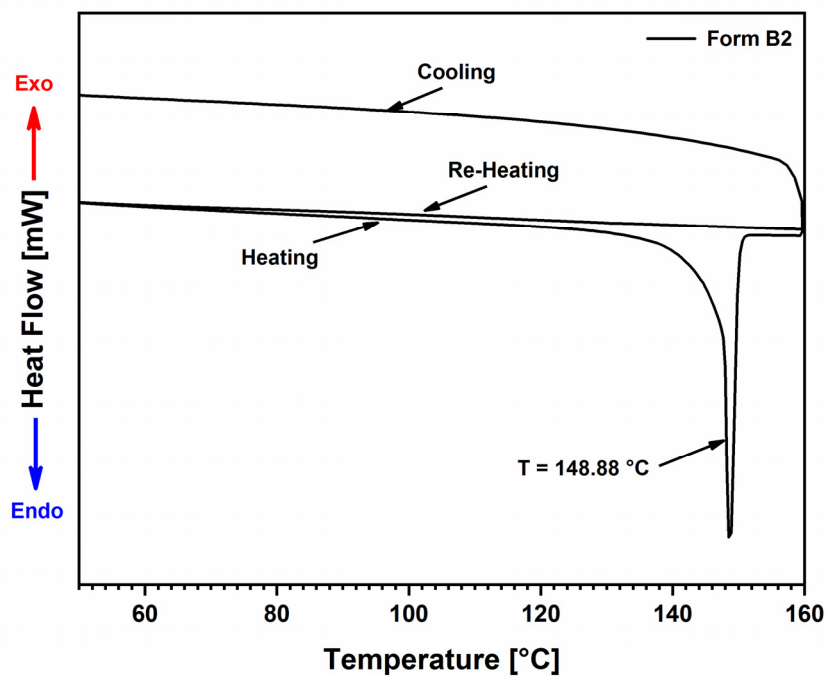
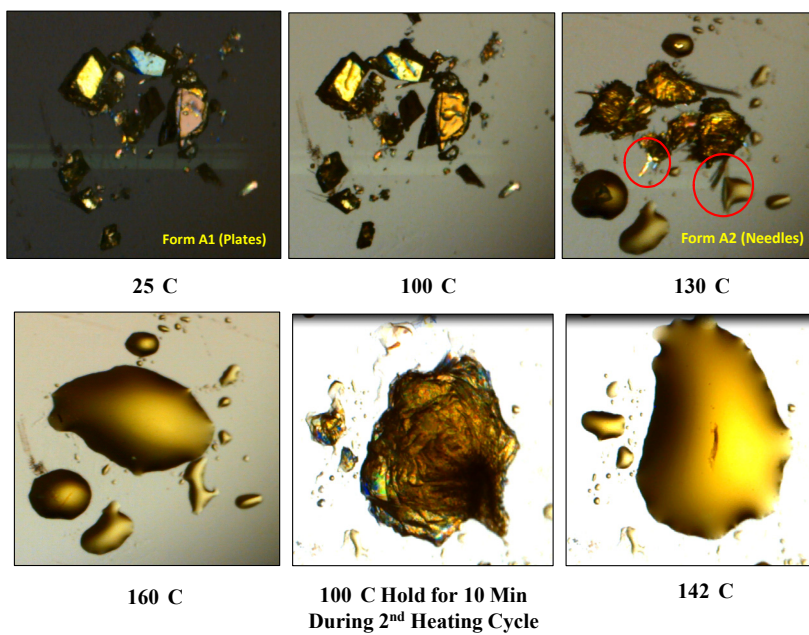
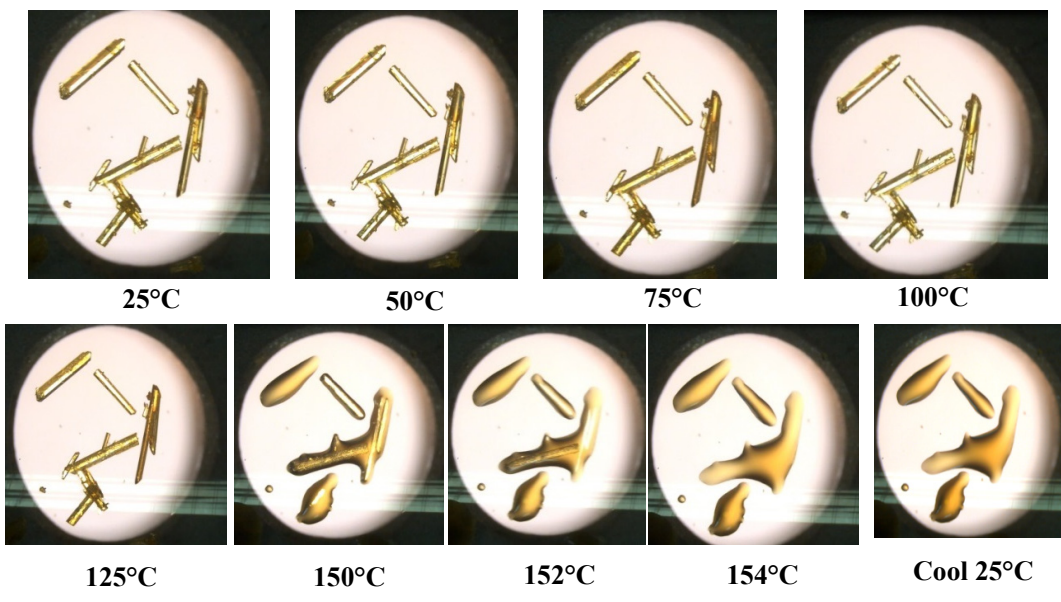


Figure S26. DSC thermogram of Form B2 crystals.



**Figure S27.** Photomicrographs of Form A1 crystals captured during its phase transition to Form A2 crystals over HSM studies.





**Figure S28.** Photomicrographs of Form A2 crystals captured during HSM study.

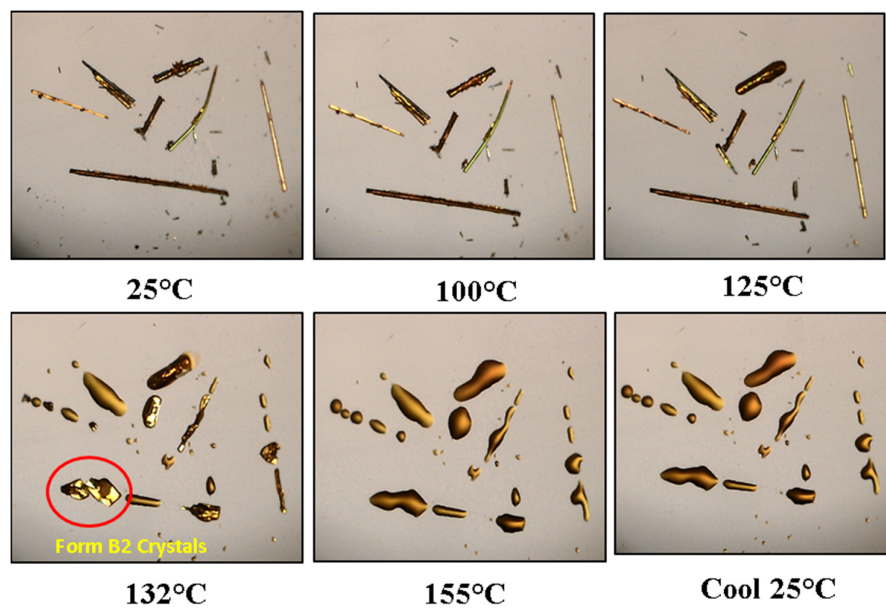


**Figure S29.** Photomicrographs of Form **B1** crystals captured during its phase transition to Form **B2** crystals over HSM studies.

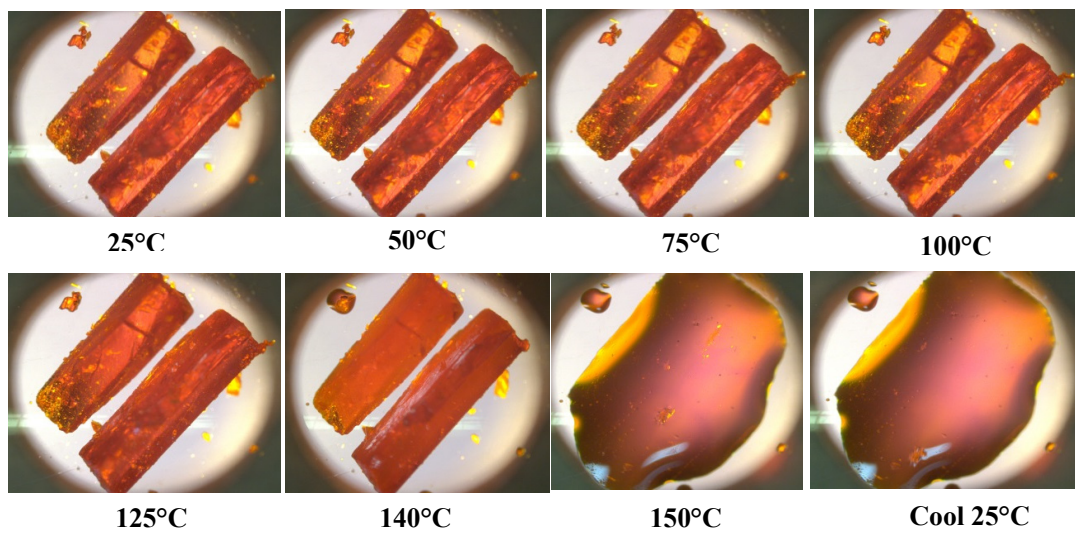


**Figure S30.** Photomicrographs of Form B2 crystals captured during HSM study.

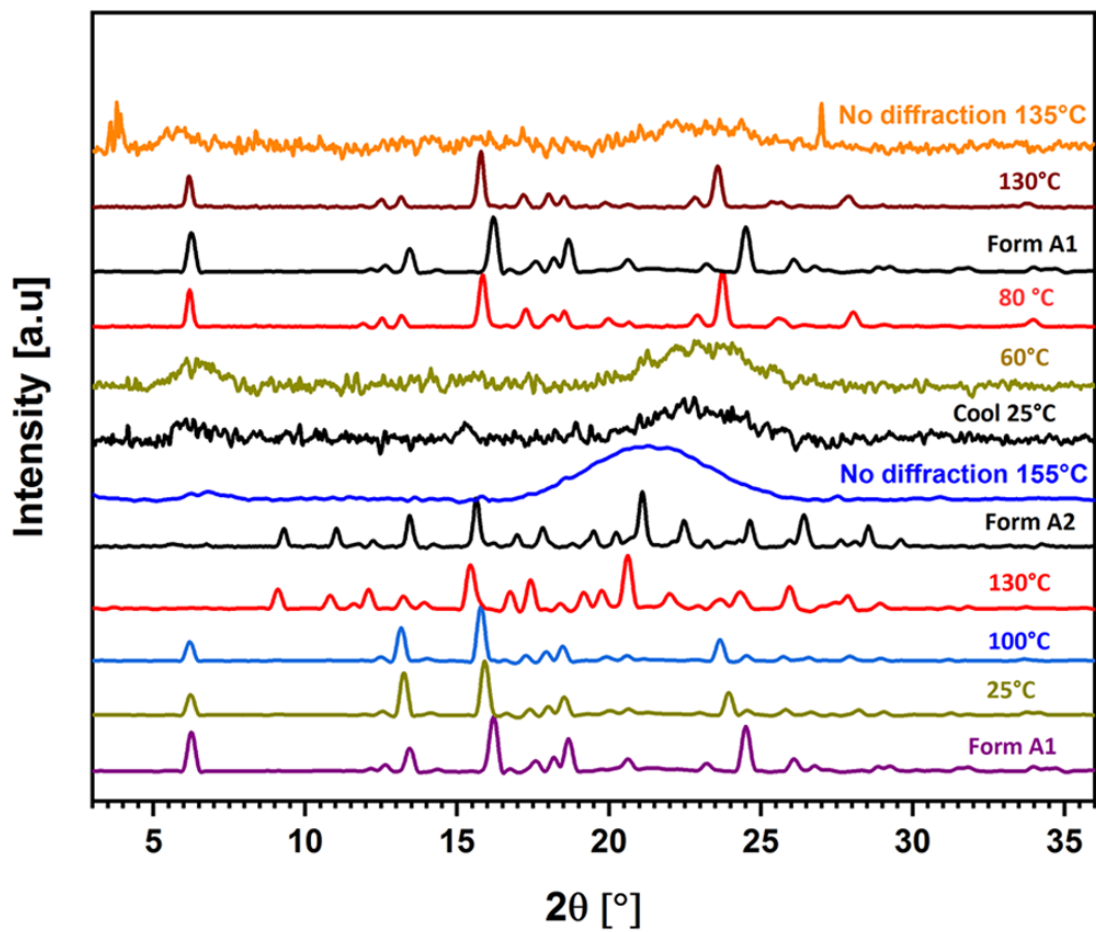
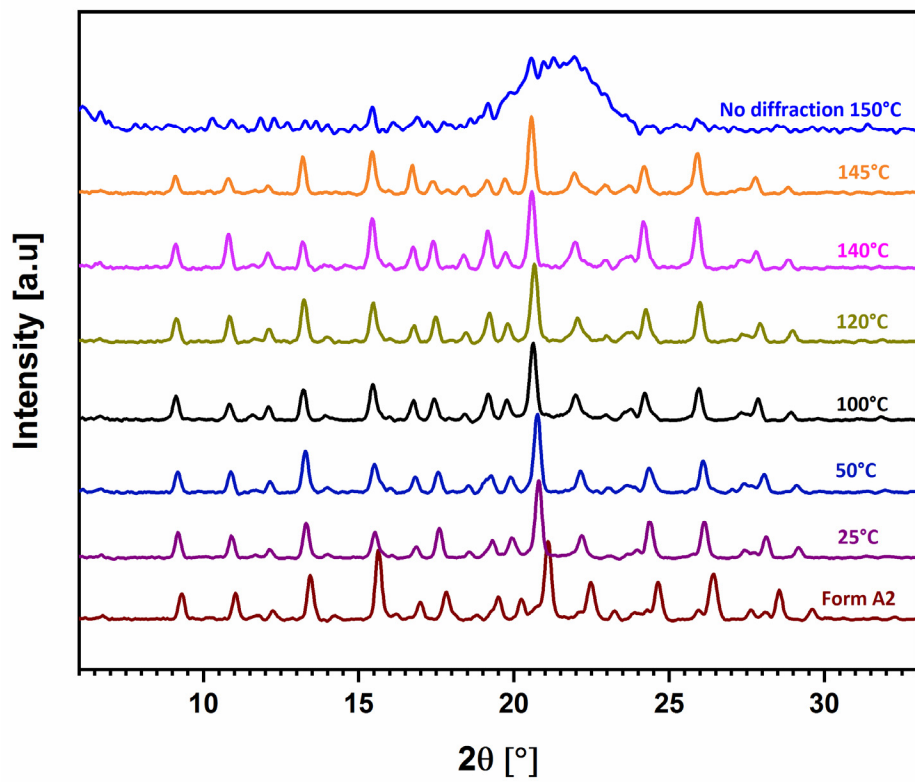
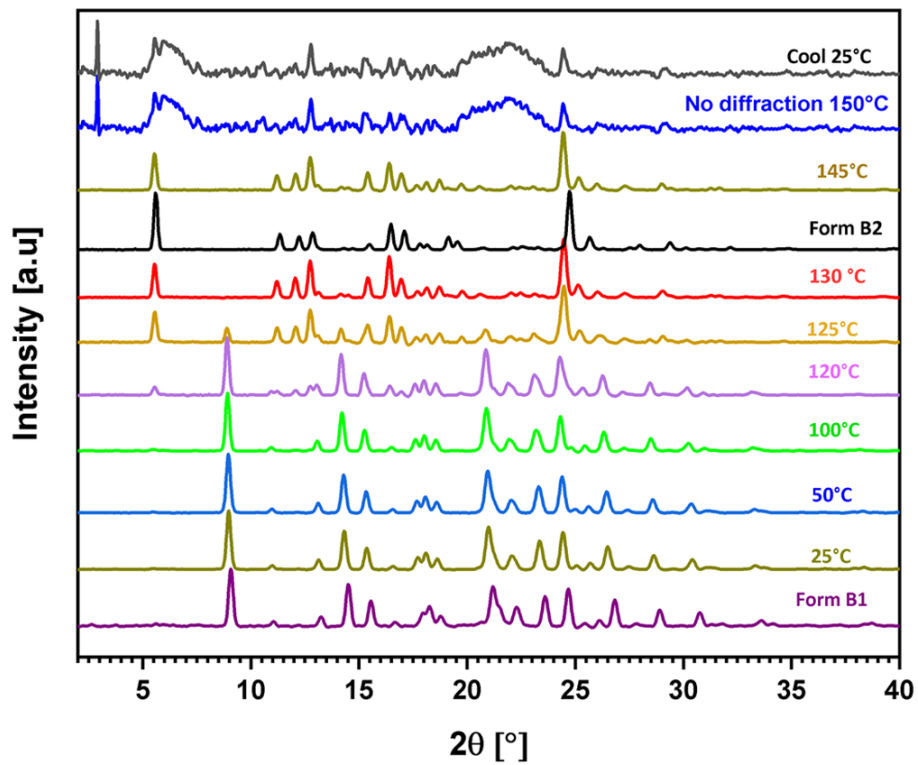


Figure S31. VT-PXRD profiles of Form A1 crystals recorded at different temperatures.



**Figure S32.** VT-PXRD profiles of Form A2 crystals recorded at different temperatures.



**Figure S33.** VT-PXRD profiles of Form **B1** crystals recorded at different temperatures.

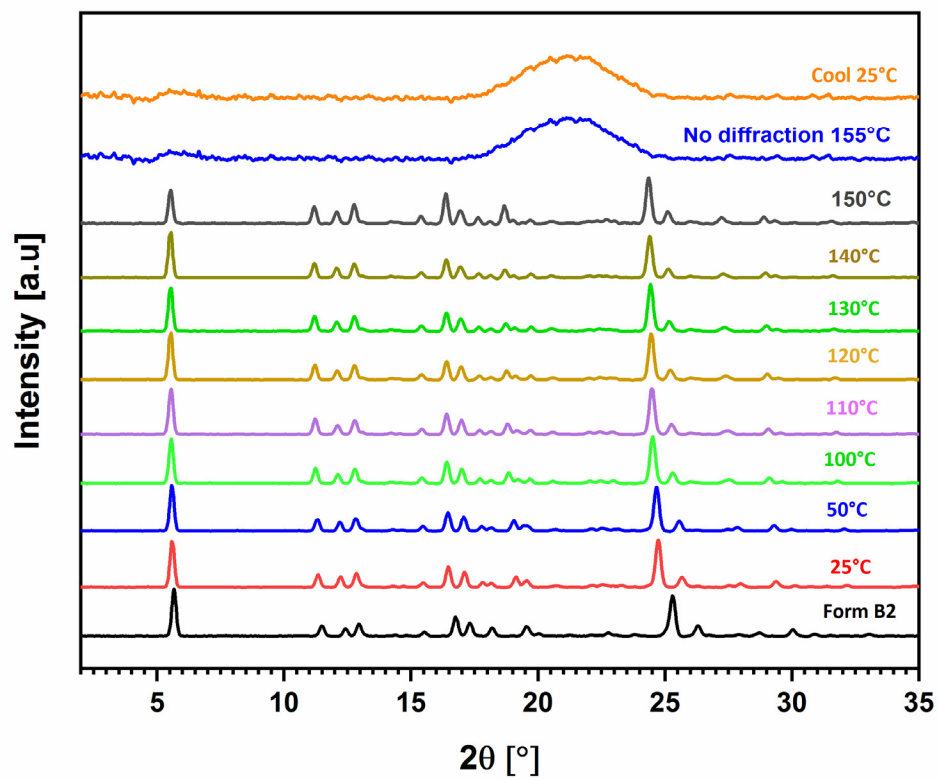


**Figure S34.** VT-PXRD profiles of Form **B2** crystals recorded at different temperatures.



**Figure S35.** Graphical representation of solvent vapour fuming experiment.



### E-Z Flipping of GFP

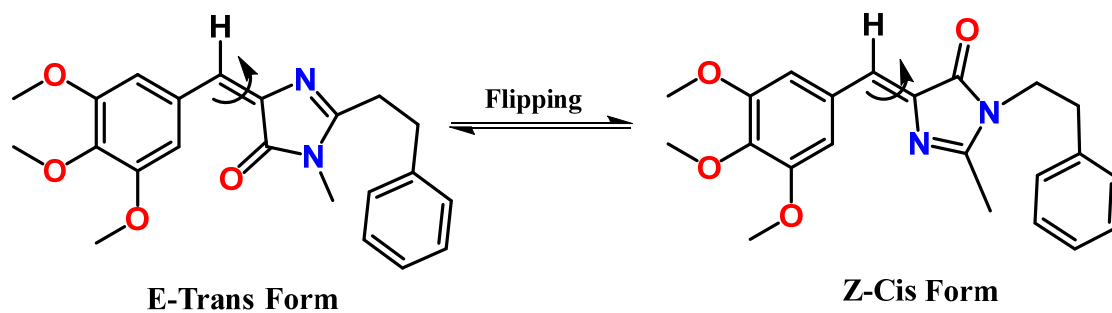


**Figure S36.** The schematic representation of E-Z flipping of GFP chromophore analog **A**.

### E-Z Flipping of GFP

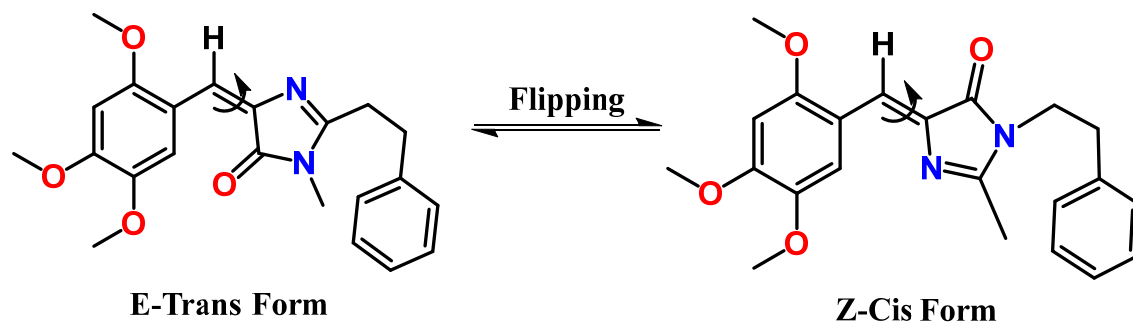


**Figure S37.** The schematic representation of E-Z flipping of GFP chromophore analog **B**.

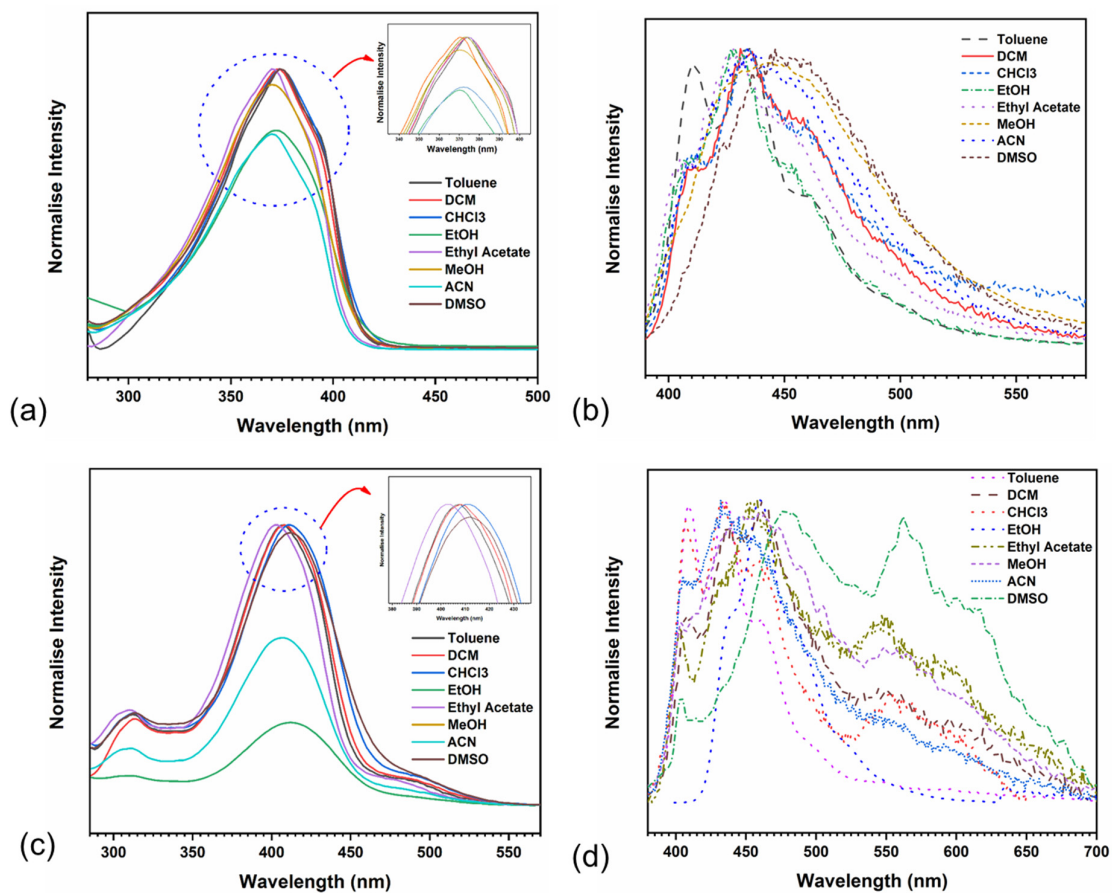


**Figure S38.** Normalized absorption (solid lines) and fluorescence (broken lines) spectra (excited at 360 nm) for, (a-b) compound **A** and (c-d) compound **B** in common organic solvents ( $C = 20 \times 10^{-5}$  M).

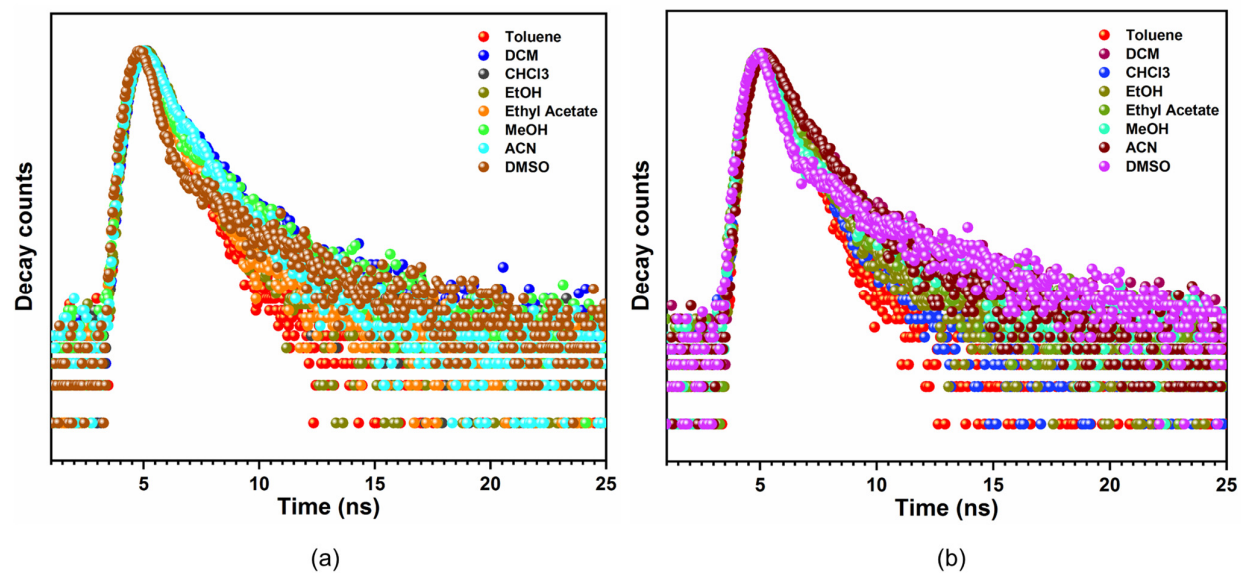


**Figure S39.** Room temperature time-resolved PL decay curves for (a) compound **A** and (b) compound **B** in common organic solvents ( $C = 20 \times 10^{-5}$  M).

**Table S10.** Absorption maxima, emission maxima, quantum yield (%), and fluorescence lifetime measurement for compound **A** in common organic solvents ( $C = 20 \times 10^{-5} \text{ M}$ ).

Sr. No	Solvent	$\lambda_{\text{ex}}$ [nm]	$\lambda_{\text{em}}$ [nm]	$\Phi_f$ (%)	$\tau_1$ [ns]	$\tau_2$ [ns]	Relative (%)		$\tau_{\text{ave}}$ [ns]
							<b>B1</b>	<b>B2</b>	
1	Toluene	374	434	0.113	0.97	2.66	94.77	5.23	1.19
2	DCM	374	433	0.018	1.07	3.96	68.48	31.52	2.89
3	CHCl <sub>3</sub>	374	434	0.014	0.90	2.76	62.98	37.02	2.09
4	EtOH	372	428	n.d	1.02	18.07	98.35	1.65	4.92
5	Ethyl Acetate	370	428	0.013	0.87	3.00	78.52	21.48	1.91
6	MeOH	370	445	n.d	0.84	3.43	56.48	43.52	2.8
7	ACN	370	435	0.014	1.06	2.98	72.14	27.86	2.06
8	DMSO	374	448	0.015	0.552	4.16	57.84	42.136	3.60

**Table S11.** Absorption maxima, emission maxima, quantum yield (%), and fluorescence lifetime measurement for compound **B** in common organic solvents ( $C = 20 \times 10^{-5} \text{ M}$ ).

Sr. No	Solvent	$\lambda_{\text{ex}}$ [nm]	$\lambda_{\text{em}}$ [nm]	$\Phi_{\text{f}}$ (%)	$\tau_1$ [ns]	$\tau_2$ [ns]	Relative (%)		$\tau_{\text{ave}}$ [ns]
							<b>B1</b>	<b>B2</b>	
1	Toluene	408	434	0.024	1.03	-	100	-	1.03
2	DCM	408	462	0.004	1.08	4.75	68.24	31.76	3.54
3	CHCl <sub>3</sub>	412	433	0.003	0.97	2.79	82.95	17.05	1.64
4	EtOH	413	464	n.d	1.05	-	100	-	1.05
5	Ethyl Acetate	403	454	0.003	0.80	3.85	64.81	35.19	3.00
6	MeOH	412	455	n.d	0.70	3.92	59.12	40.88	3.26
7	ACN	406	433	0.003	1.23	5.21	83.87	16.13	3.02
8	DMSO	412	482	0.003	0.58	4.96	49.16	50.84	4.52

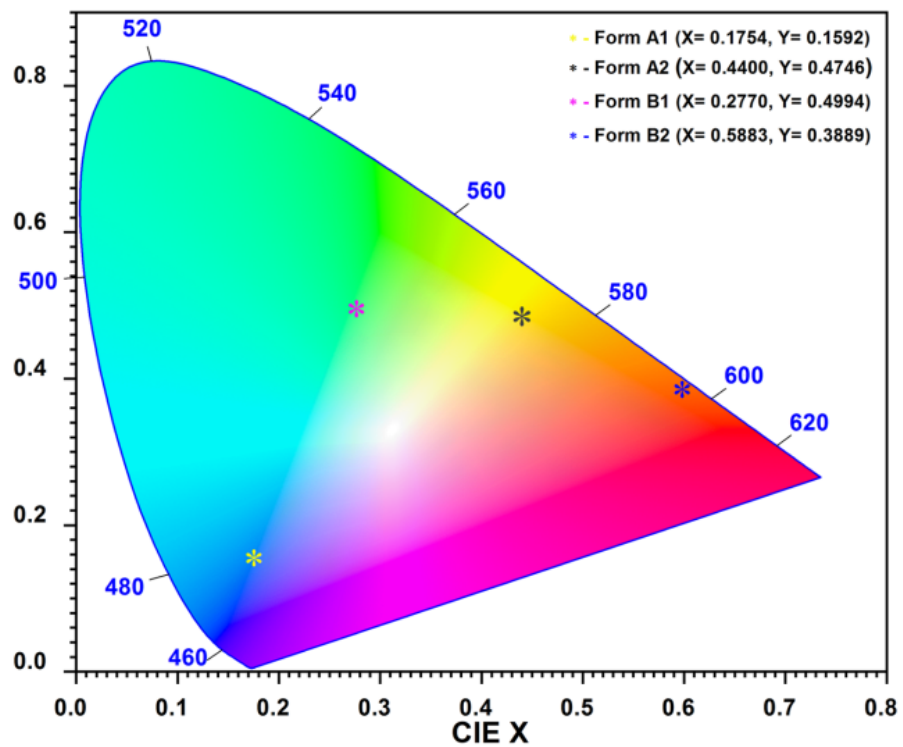


**Figure S40.** The CIE coordinates position on chromaticity for emission of the polymorph A1 (yellow star), A2 (green star), B1 (pink star) and B2 (blue star) in the crystalline state.

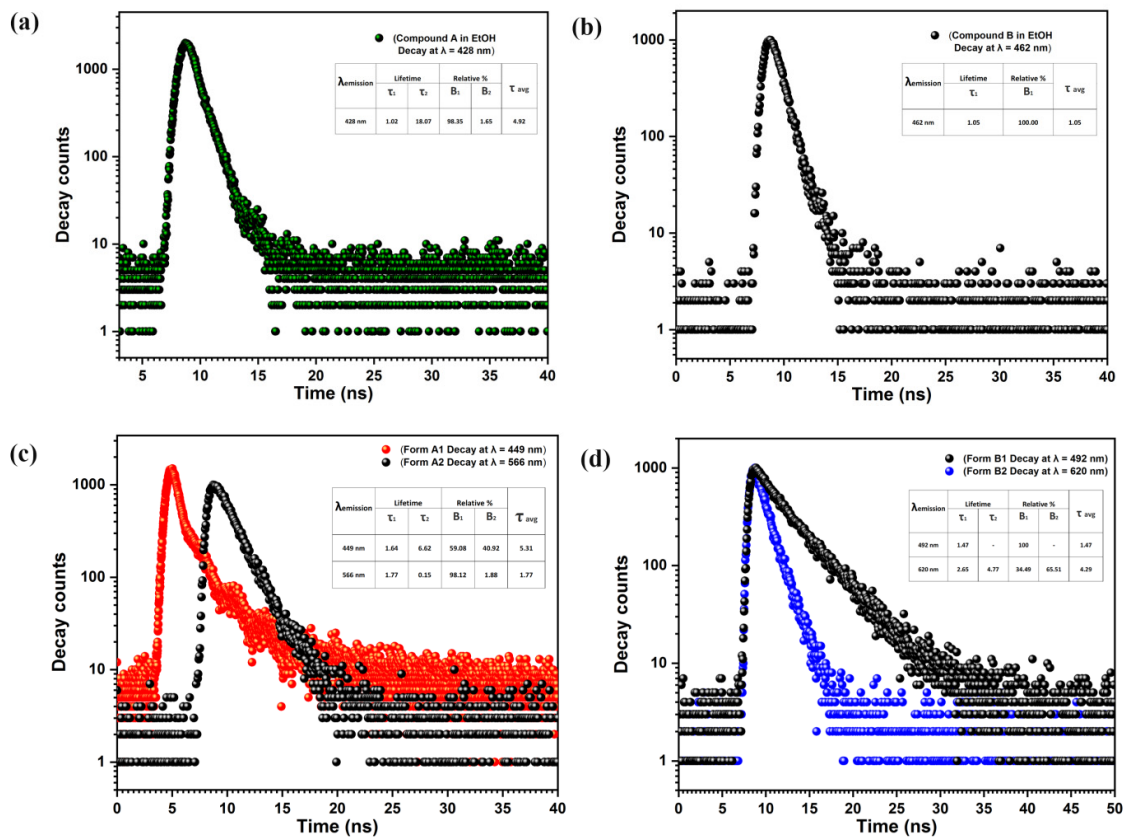


**Figure S41.** Room temperature time-resolved PL decay curves for compound **A** and **B** (a) **A** in Ethanol solution, (b) **B** in Ethanol solution, (c) for polymorphs of **A** and (d) for polymorphs of **B**.

**Table S12.** Absorption maxima, emission maxima, quantum yield (%), and fluorescence lifetime measurement for the polymorphs of compound **A** and **B** in the solid-state.

Sr.No	$\lambda_{ex}$ [nm]	$\lambda_{em}$ [nm]	Absolute $\Phi_f$ (%)	$\tau_1$ [ns]	$\tau_2$ [ns]	Relative (%)		$\tau_{ave}$ [ns]	$K_r$ ( $10^7s^{-1}$ )	$K_{nr}$ ( $10^7s^{-1}$ )
						<b>a</b> <sub>1</sub>	<b>a</b> <sub>2</sub>			
Form A1	400	449	5.24	1.64	6.62	59.08	40.92	5.31	0.01	1.89
Form A2	402	566	4.89	1.77	0.15	98.12	1.88	1.77	2.76	5.74
Form B1	456	492	2.93	1.47	-	100	-	1.47	2.0	6.90
Form B2	406	620	7.06	2.65	4.77	34.49	65.51	4.29	1.65	2.34



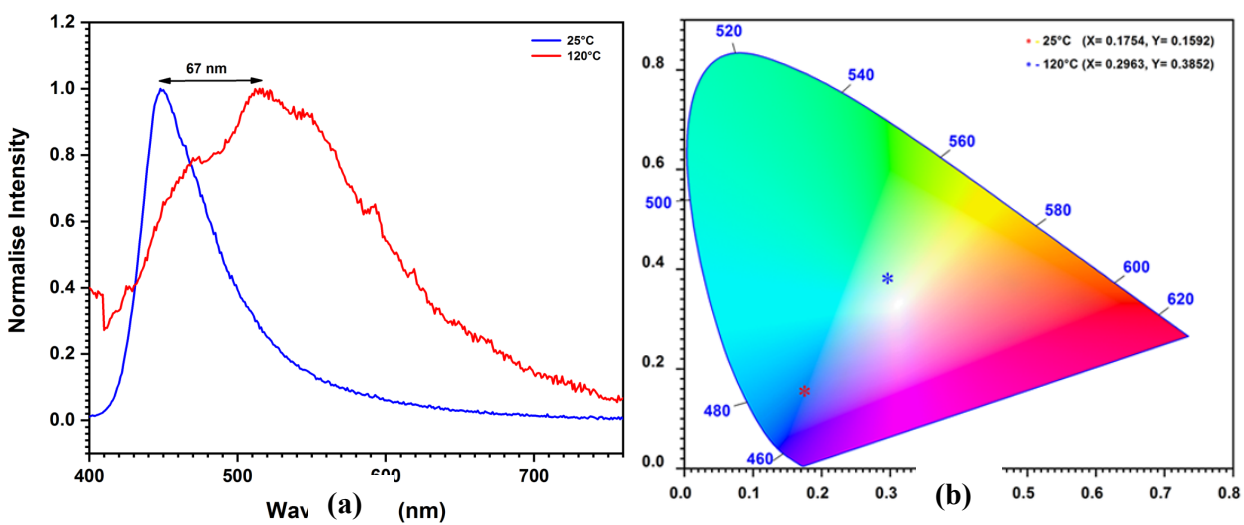


**Figure S42.** (a) Normalized fluorescence spectra (excited at 360 nm) for Form A1 recorded at different temperatures, (b) CIE coordinates position on chromaticity for emission of Form A1 at 25°C (red star) and at 100°C (blue star) in the crystalline state.

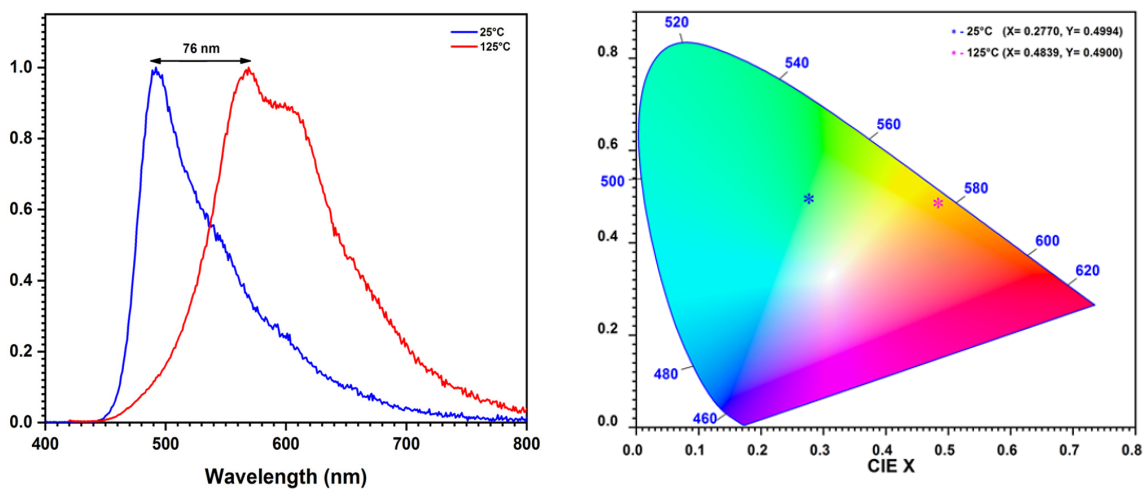


**Figure S43.** (a) Normalized fluorescence spectra (excited at 360 nm) for Form **B1** recorded at different temperatures, (b) CIE coordinates position on chromaticity for emission of Form **B1** at 25°C (blue star) and at 125°C (pink star) in the crystalline state.



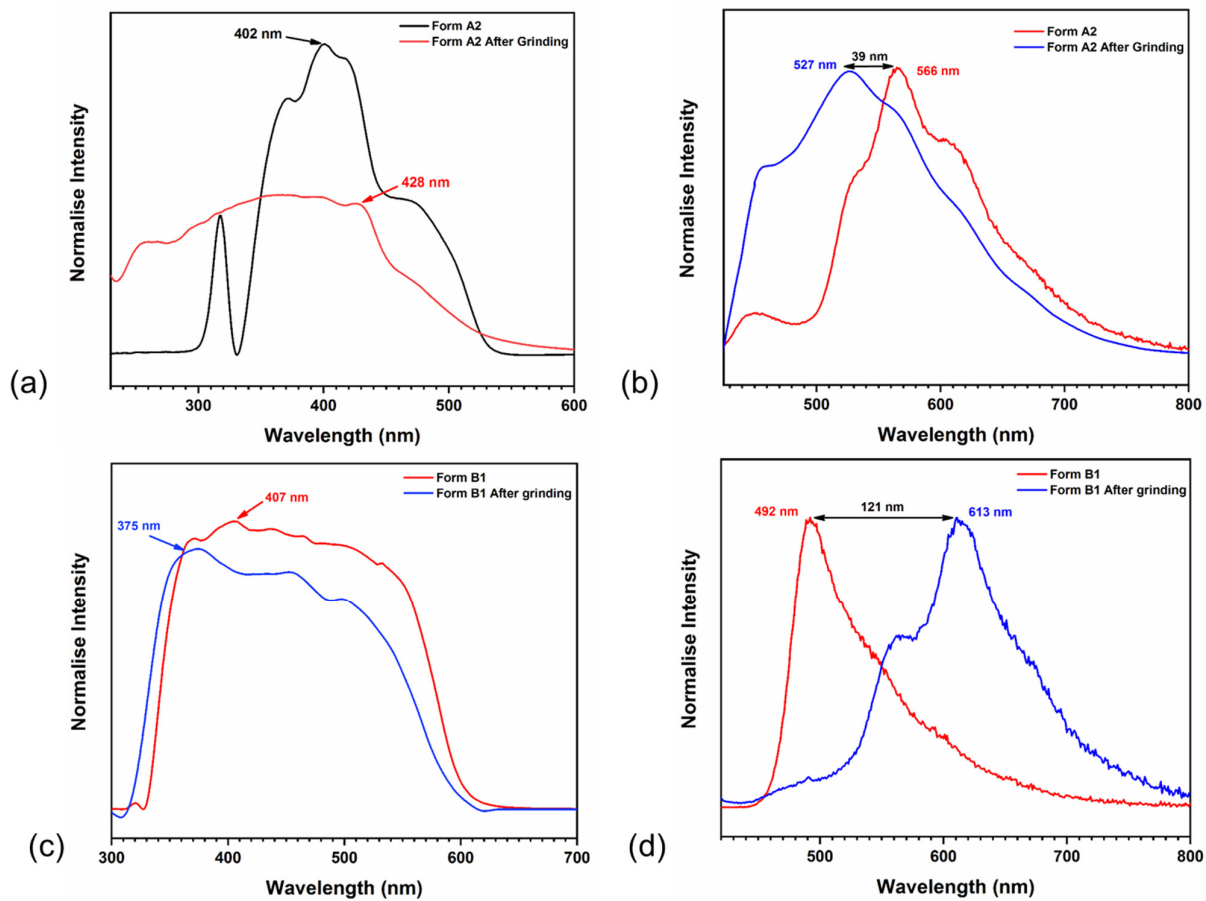


**Figure S45.** Normalized solid-state absorption and fluorescence spectra (excited at 360 nm) for (a-b) Form A2 and (c-d) for Form B1 respectively.

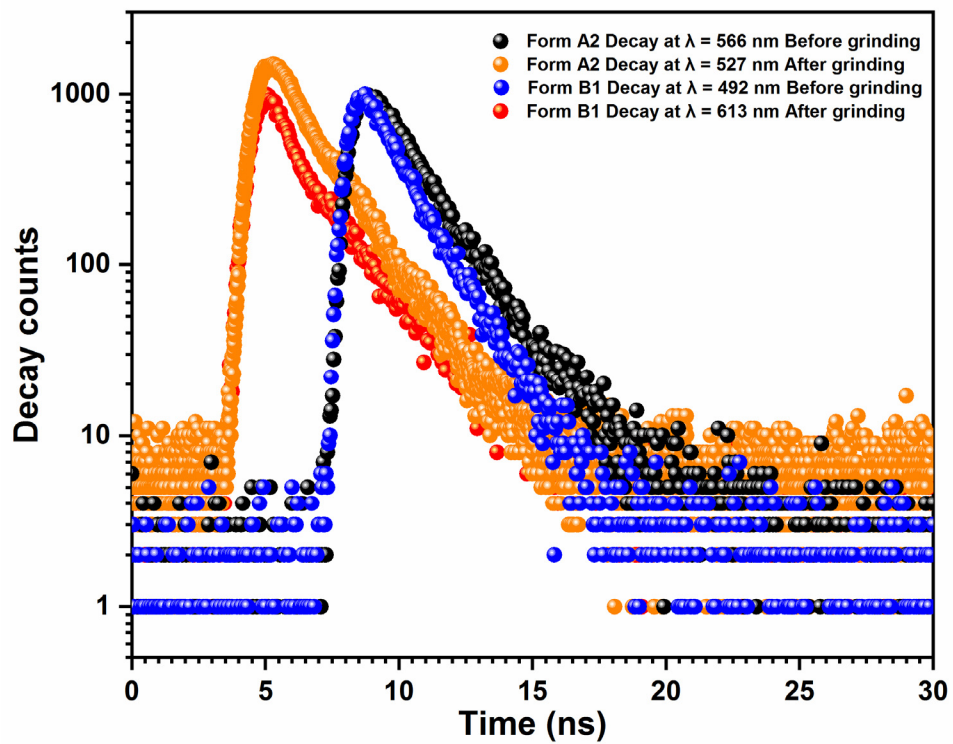


**Figure S46.** Room temperature time-resolved PL decay curves for Form A2 and Form B1, before and after grinding.

**Table S13.** Absorption maxima, emission maxima, quantum yield (%), and fluorescence lifetime measurement for Form **A2** and Form **B1** in the solid-state.

Solvent	$\lambda_{\text{ex}}$ [nm]	$\lambda_{\text{em}}$ [nm]	$\Phi_f$ (%)	$\tau_1$ [ns]	$\tau_2$ [ns]	Relative (%)		$\tau_{\text{ave}}$ [ns]	$K_r$ ( $10^7\text{s}^{-1}$ )	$K_{\text{nr}}$ ( $10^7\text{s}^{-1}$ )
						B1	B2			
Form A2 Before grinding	402	566	4.89	1.77	0.15	98.12	1.88	1.77	2.76	5.74
Form A2 After grinding	428	527	3.37	0.85	1.58	81.61	18.39	1.07	3.14	9.63
Form B1 Before grinding	456	492	2.93	1.47	-	100	-	1.47	2.0	6.90
Form B1 After grinding	375	613	4.21	0.95	2.74	41.55	58.45	2.39	1.76	4.22

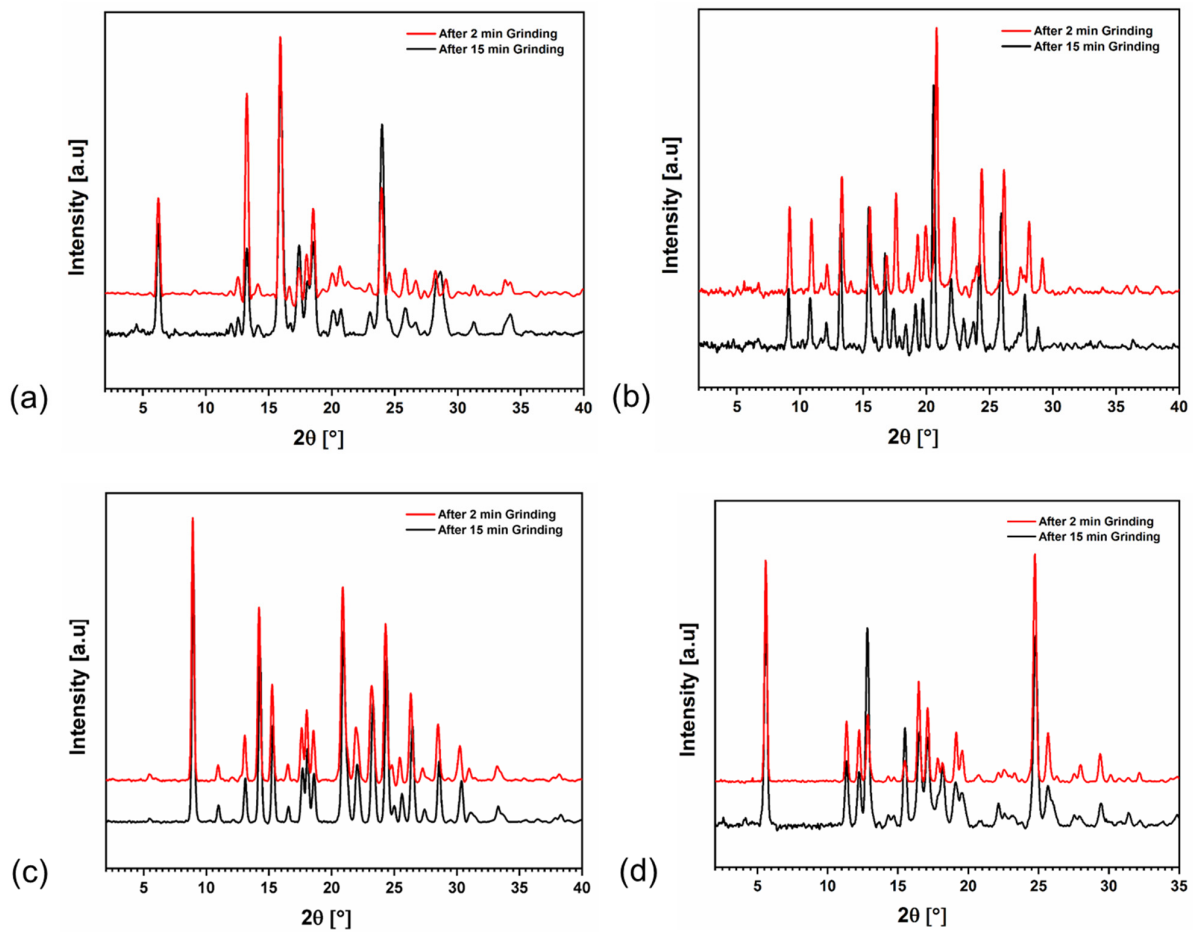


**Figure S47.** Overlay of powder X-ray diffraction patterns of (a) Form A1, (b) Form A2, (c) Form B1 and (d) Form B2.

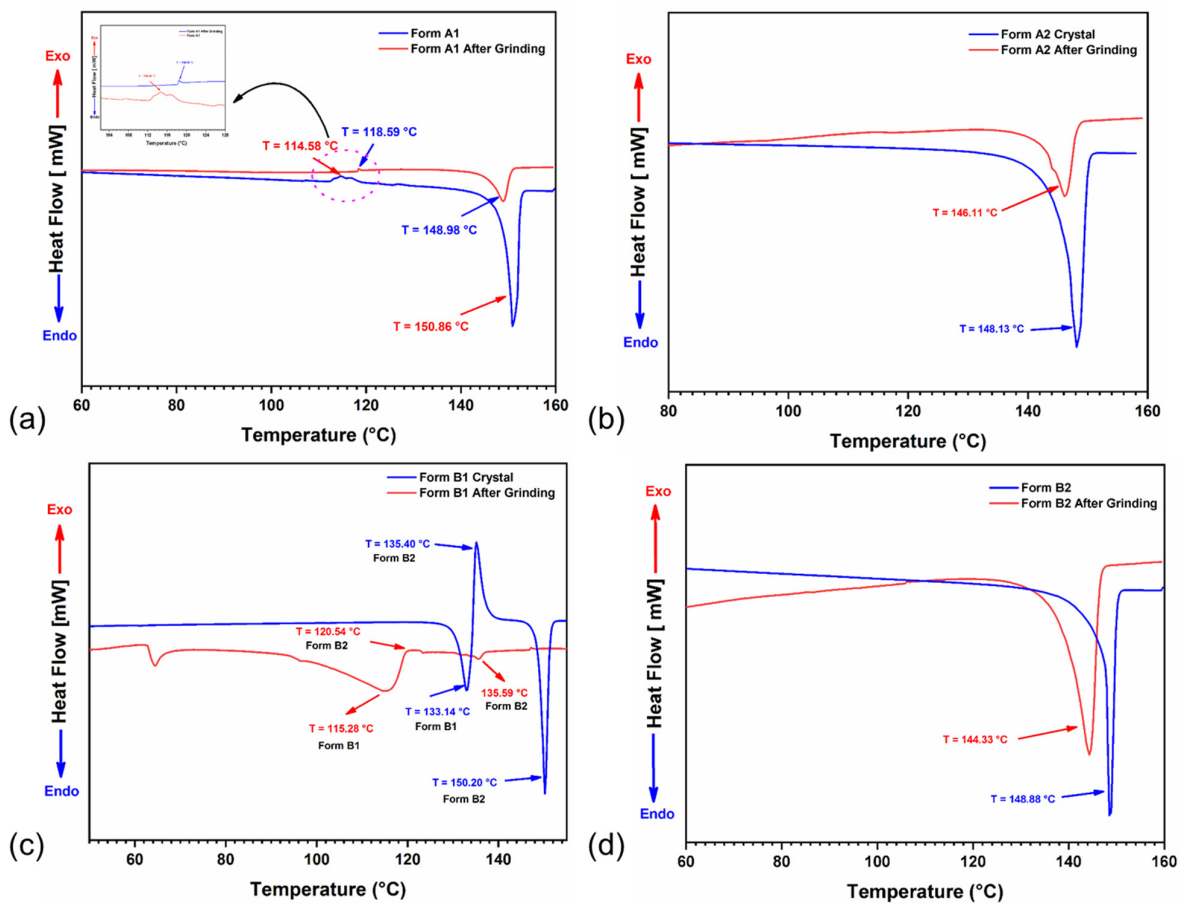


**Figure S48.** Overlay of DSC thermograms for, (a) Form A1, (b) Form A2, (c) Form B1 and (d) Form B2 in crystalline and powdered state.



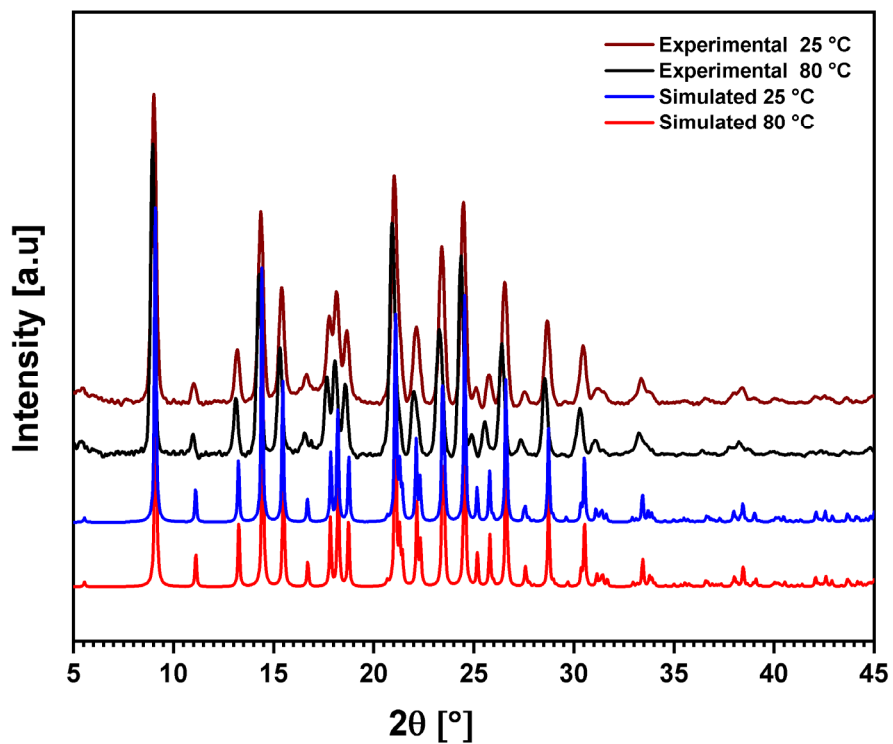


**Figure S49.** Overlay of experimental and calculated powder X-ray diffraction patterns of Form **B1** recorded at different temperatures.

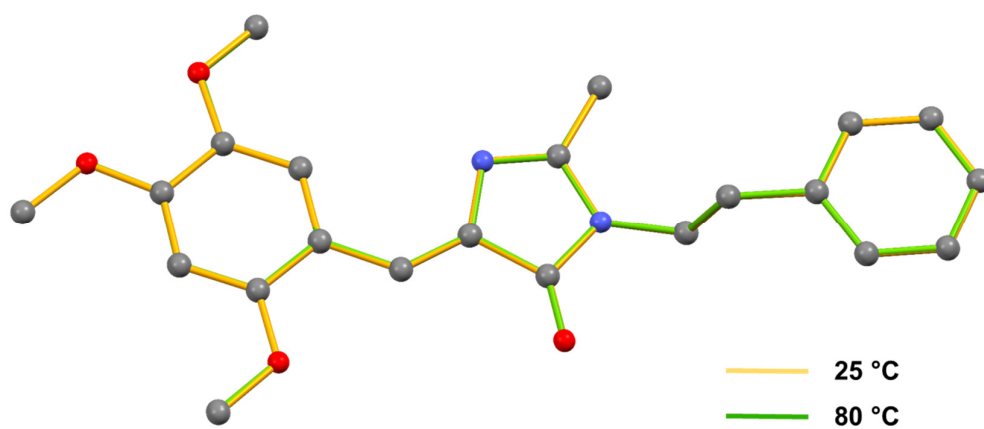


**Figure S50.** Structure overlay of Form **B1** collected at 25 °C (yellow) and 80 °C (green).

## Calculations of Photophysical Parameters

The photophysical parameters were calculated using following equations:

$$\tau_{\text{ave}} = a_1 (\tau_1)^2 + a_2 (\tau_2)^2 / a_1 \tau_1 + a_2 \tau_2$$

$$K_r = \Phi_F / \tau_F$$

$$K_{nr} = 1 / (\tau_F) - K_r$$

where,

$K_r$  = Radiative rate constant of fluorescence

$K_{nr}$  = Non-radiative rate constant of fluorescence

$\Phi_F$  = Fluorescence quantum yield

$\tau_F$  = Fluorescence lifetime

## Bandgap calculations:

The bandgap calculation is carried out by the following Davis-Mott relation (tau-plot),

$$\alpha h\nu = A (h\nu - E_g)^n$$

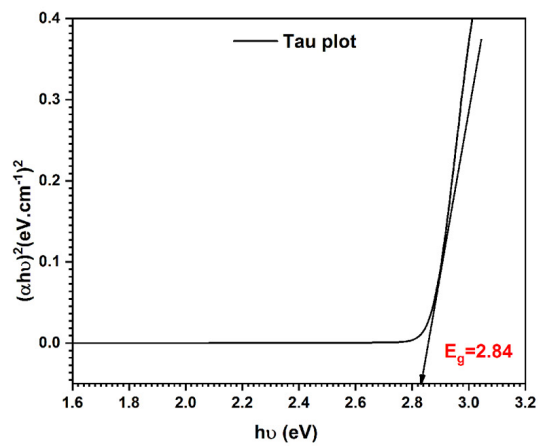
Where,

A = Energy independent constant

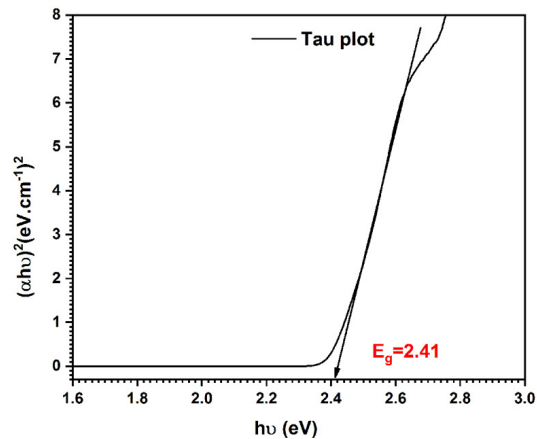
$E_g$  = Optical energy gap

$\alpha$  = Absorption coefficient

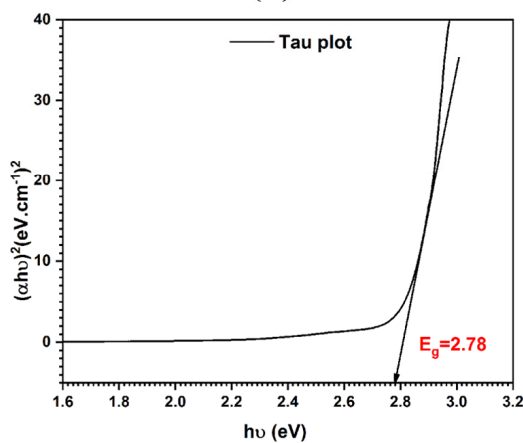
n - Denotes the nature of transition



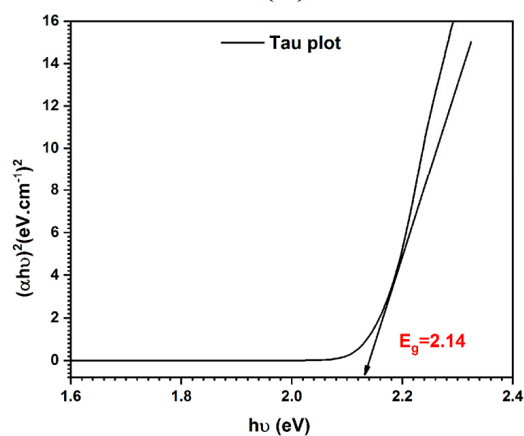
(a)



(b)



(c)



(d)

**Figure S51.** Tauc plot of UV-visible absorption data for the calculation of band-gap energy of all the polymorphs of **A** and **B** (a) Form A1, (b) Form A2, (c) Form B1 and (d) Form B2.

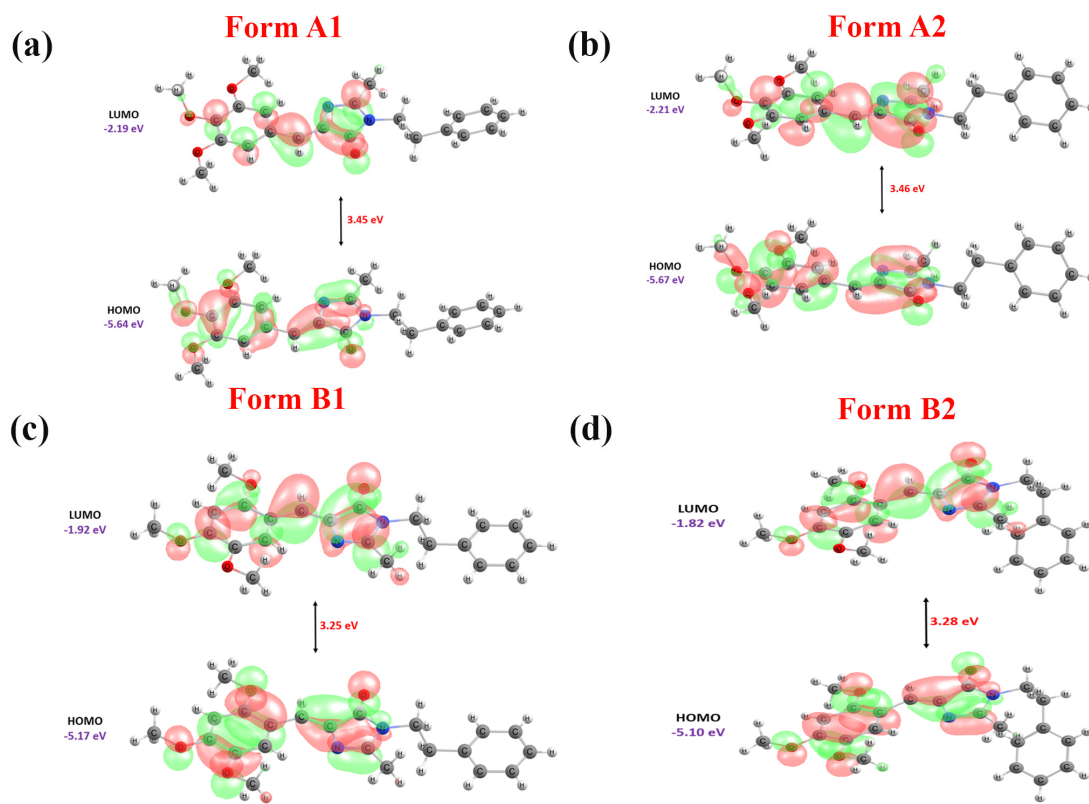


**Figure S52.** Frontier molecular orbitals and their corresponding energy levels are calculated using the Gaussian 09 program by employing the B3LYP/6-311<sup>++</sup>G(d,p) level of theory. (a) Form A1, (b) Form A2, (c) Form B1 and (d) Form B2.

**Table S14.** Band gap and transition values corresponding to the  $\lambda_{\max}$ . ( $f$ = oscillator strength)

Name	Experimental Tau plot (eV)	HOMO-LUMO gap		TD-DFT [ $\lambda_{\max}$ ]	
		B3LYP (eV)	B97D3 (eV)	B3LYP	B97D3
Form A1	2.84	3.45	2.21	3.30 eV 375.37 nm HOMO to LUMO $f=0.5884$	2.94 eV 421.60 nm HOMO to LUMO $f=0.4182$
Form A2	2.41	3.46	2.22	3.30 eV 374.82 nm HOMO to LUMO $f=0.5585$	2.91 eV 426.20 nm HOMO to LUMO $f=0.4455$
Form B1	2.78	3.25	2.04	3.06 eV 404.48 nm HOMO to LUMO $f=0.5964$	2.68 eV 463.09 nm HOMO to LUMO $f=0.3525$
Form B2	2.14	3.28	2.07	3.10 eV 399.84 nm HOMO to LUMO $f=0.5798$	2.72 455.41 nm HOMO to LUMO $f=0.3478$

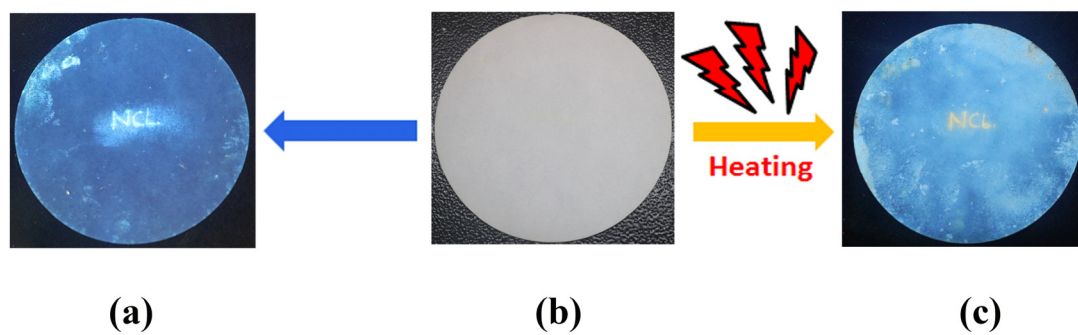


**Figure S53.** Ethanol-based anti-counterfeiting ink was prepared from Form A1 and observed under the (a) UV light (b) visible light and (c) UV light after heating to 140°C.

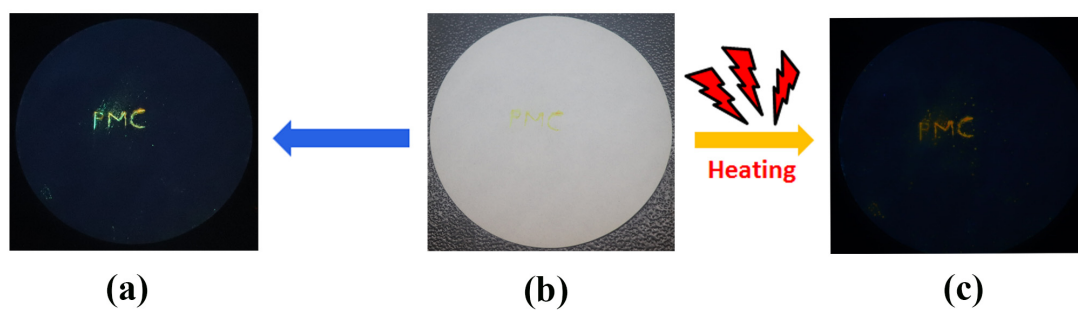


**Figure S54.** Ethanol-based anti-counterfeiting ink prepared from Form B1 under the (a) UV light, (b) visible light, and (c) UV light after heating to 140°C.

## References

- 1 Bruker. APEX3, SAINT-Plus and SADABS; Bruker AXS Inc: Madison, Wisconsin, USA, 2016.
- 2 G. M. Sheldrick, *Acta Crystallogr. Sect. A Found. Crystallogr.*, 2008, **64**, 112–122.
- 3 G. M. Sheldrick, *Acta Crystallogr. Sect. C Struct. Chem.*, 2015, **C71**, 3–8.
- 4 L. J. Farrugia, *J. Appl. Crystallogr.*, 2012, **45**, 849–854.
- 5 C. F. Macrae, I. Sovago, S. J. Cottrell, P. T. A. Galek, P. McCabe, E. Pidcock, M. Platings, G. P. Shields, J. S. Stevens, M. Towler and P. A. Wood, *J. Appl. Crystallogr.*, 2020, **53**, 226–235.
- 6 A. L. Spek, *J. Appl. Crystallogr.*, 2003, **36**, 7–13.
- 7 A. Gavezzotti, *New J. Chem.*, 2011, **35**, 1360–1368.
- 8 A. Gavezzotti, *Acc. Chem. Res.*, 1994, **27**, 309–314.
- 9 A. Gavezzotti and G. Filippini, *J. Phys. Chem.*, 1994, **98**, 4831–4837.
- 10 M. A. Spackman and D. Jayatilaka, *CrystEngComm*, 2009, **11**, 19–32.
- 11 S. K. Wolff, D. J. Grimwood, J. J. McKinnon, M. J. Turner, D. Jayatilaka and M. A. Spackman, Crystal Explorer 3.0. University of Western Australia, Perth, 2012.
- 12 M. A. Spackman and J. J. McKinnon, *CrystEngComm*, 2002, **4**, 378–392.
- 13 M. J. Turner, S. P. Thomas, M. W. Shi, D. Jayatilaka and M. A. Spackman, *Chem. Commun.*, 2015, **51**, 3735–3738.
- 14 N. Kourkoumelis, *Powder Diffr.*, 2013, **28**, 137–48.
- 15 M. J. Frisch, GAUSSIAN09; Revision D.01; Gaussian Inc: Wallingford, CT, USA, 2013.
- 16 A. D. Becke, *J. Chem. Phys.*, 1993, **98**, 5648–5652.
- 17 S. Grimme, *J. Comp.*, 2006, **27**, 1787–1799.